

1 **Tropospheric aerosol hygroscopicity in China**

2 Chao Peng,¹ Yu Wang,² Zhijun Wu,² Lanxiadi Chen,^{1,6} Ru-Jin Huang,³ Weigang Wang,⁴ Zhe
3 Wang,⁵ Weiwei Hu,¹ Guohua Zhang,¹ Maofa Ge,^{4,6,7} Min Hu,² Xinming Wang,^{1,6,7} Mingjin
4 Tang^{1,6,7,*}

5

6 1 State Key Laboratory of Organic Geochemistry, Guangdong Key Laboratory of Environmental Protection and
7 Resources Utilization, and Guangdong-Hong Kong-Macao Joint Laboratory for Environmental Pollution and
8 Control, Guangzhou Institute of Geochemistry, Chinese Academy of Sciences, Guangzhou 510640, China

9 ² State Key Joint Laboratory of Environmental Simulation and Pollution Control, College of Environmental
10 Sciences and Engineering, Peking University, Beijing 100871, China

11 ³ State Key Laboratory of Loess and Quaternary Geology, Center for Excellence in Quaternary Science and
12 Global Change, and Key Laboratory of Aerosol Chemistry and Physics, Institute of Earth Environment,
13 Chinese Academy of Sciences, 710061 Xi'an, China

14 ⁴ State Key Laboratory for Structural Chemistry of Unstable and Stable Species, Beijing National Laboratory
15 for Molecular Sciences (BNLMS), CAS Research/Education Center for Excellence in Molecular Sciences,
16 Institute of Chemistry, Chinese Academy of Sciences, Beijing 100190, China

17 ⁵ Division of Environment and Sustainability, The Hong Kong University of Science and Technology, Hong
18 Kong, China

19 ⁶ University of Chinese Academy of Sciences, Beijing 100049, China

20 ⁷ Center for Excellence in Regional Atmospheric Environment, Institute of Urban Environment, Chinese
21 Academy of Sciences, Xiamen 361021, China

22

23 * Correspondence: Mingjin Tang (mingjintang@gig.ac.cn)

24

25

26 **Abstract**

27 Hygroscopicity largely determines phase state, chemical reactivity, optical properties and
28 cloud nucleation activities of aerosol particles, thus significantly affecting their impacts on
29 visibility, atmospheric chemistry and climate. In the last twenty years a large number of field
30 studies have investigated hygroscopicity of tropospheric aerosols in China under sub- and super-
31 saturated conditions. Aerosol hygroscopicity measurements in China are reviewed in this paper: 1)
32 a comprehensive summary and critical discussion of aerosol hygroscopicity measurements in
33 China is provided; 2) available measurement data are compiled and presented under a consistent
34 framework to enhance their accessibility and usability; 3) current knowledge gaps are identified,
35 and an outlook which could serve as guidelines for planning future research is also proposed.

36

37

38 **1 Introduction**

39 In the last few decades, rapid industrial, economic and social developments in China have
40 caused large emissions of gaseous and particulate pollutants into the troposphere (Li et al., 2017a),
41 where they are mixed with gases and aerosols from natural sources. Under unfavourable
42 meteorological conditions (i.e. when air is stagnant and stable), severe air pollution occurs, due to
43 accumulation of primary pollutants and more importantly, formation of secondary pollutants (Zhu
44 et al., 2011; He et al., 2014; Zhang et al., 2015; An et al., 2019; Lu et al., 2019; Zhang et al., 2019c).
45 During severe air pollution events, $PM_{2.5}$ could exceed a few hundred $\mu g m^{-3}$ (Guo et al., 2014;
46 Huang et al., 2014) and O_3 could reach up to >200 ppbv (Wang et al., 2017b). The concept of air
47 pollution complex has been proposed to describe the complexity of air pollution in China,
48 characterized by complex sources and complex interactions of a myriad of gaseous and particulate
49 pollutants (Zhu et al., 2011; Lu et al., 2019; Chu et al., 2020). Thanks to the implementation of
50 effective air pollution control measures, substantial decrease in $PM_{2.5}$ has occurred nationwide in
51 the last several years (Zhang et al., 2019b); however, slight but significant increase in O_3 has been
52 observed in many regions during the same period (Li et al., 2019a; Lu et al., 2020), revealing the
53 complexity and difficulty in synergistic control of $PM_{2.5}$ and O_3 .

54 Hygroscopicity, one of the most important physicochemical properties of aerosols, determines
55 the amount of water associated with aerosol particles under ambient conditions (mainly relative
56 humidity, and temperature to a less extent) and significantly affects their environmental and
57 climatic impacts (Kreidenweis and Asa-Awuku, 2014; Tang et al., 2019). Hygroscopicity is
58 referred to hygroscopic properties under subsaturated conditions from a specific view, while from
59 a general view, it is referred to both hygroscopic properties under subsaturated conditions and
60 cloud condensation nucleation (CCN) activities under supersaturated conditions. Due to their

61 hygroscopicity, aerosol particles will take up water (i.e. hygroscopic growth) and lead to increase
62 in particle mass and size (Kreidenweis and Asa-Awuku, 2014; Tang et al., 2016; Wu et al., 2018b;
63 Tang et al., 2019). Therefore, hygroscopicity largely determines optical properties of aerosols and
64 as a result their impacts on visibility and direct radiative forcing under subsaturated conditions
65 (Titos et al., 2016; Zhao et al., 2019); on the other hand, hygroscopicity is also closely linked to
66 CCN activities of aerosols and thus their abilities to **form** cloud droplets under supersaturated
67 conditions (Kreidenweis and Asa-Awuku, 2014; Farmer et al., 2015; Tang et al., 2016), thereby
68 having important implications for their indirect radiative forcing (Dusek et al., 2006; McFiggans
69 et al., 2006; Farmer et al., 2015). Furthermore, hygroscopicity determines aerosol liquid water
70 content (ALWC) and thus phase state, acidity and chemical reactivities of aerosols (Bertram and
71 Thornton, 2009; Liu et al., 2017; Tang et al., 2017; Wu et al., 2018b), playing critical roles in
72 secondary aerosol formation as well as removal and production of trace gases. In addition,
73 hygroscopic growth measurements can provide valuable insights into mixing states of aerosols
74 (Swietlicki et al., 2008; Riemer et al., 2019). Due to its importance, tropospheric aerosol
75 hygroscopicity has been investigated in China by a number of field studies in the last 10-20 years,
76 as reviewed in this paper.

77 Swietlicki et al. (Swietlicki et al., 2008) summarized and analyzed hygroscopic properties of
78 ambient aerosols measured using H-TDMA (Hygroscopic Tandem Differential Mobility Analyser)
79 prior to September 2007, when ambient aerosol hygroscopicity was seldom explored in China. The
80 effects of hygroscopicity on aerosol light scattering have been reviewed and summarized on the
81 global scale (Titos et al., 2016; Burgos et al., 2019), and a very recent paper also briefly
82 summarizes aerosol light scattering enhancement studies in China (Zhao et al., 2019). A book
83 chapter (Kreidenweis and Asa-Awuku, 2014) discussed in brief hygroscopic growth and light

84 scattering enhancement of ambient aerosols, but only a few measurements conducted in China
85 were included. In addition, a recent paper (Tang et al., 2019) has reviewed aerosol hygroscopicity
86 measurement techniques, **but it only discussed several exemplary studies to illustrate how specific**
87 **techniques can help us better understand tropospheric aerosol hygroscopicity.**

88 In the last few decades, a number of field studies have investigated tropospheric aerosol
89 hygroscopicity in China. However, a general overview of spatial and temporal variation of aerosol
90 hygroscopicity in China is yet to be provided, and the dependence of aerosol hygroscopicity on
91 aerosol composition, mixing state, and etc. has not been fully elucidated. In this paper we provide
92 a comprehensive review of hygroscopic properties of ambient aerosols measured using H-TDMA
93 in China; in addition, CCN activities of tropospheric aerosols measured in China are also reviewed
94 and discussed. Via using the single hygroscopicity parameter (κ), we attempt to reconcile
95 hygroscopic properties examined at $<100\%$ RH (relative humidity) with CCN activities measured
96 at $>100\%$ RH. A number of studies measured light scattering enhancement factors, $f(RH)$, of
97 ambient aerosols in China (Zhao et al., 2019), but most of these studies are not included herein for
98 two reasons: 1) $f(RH)$ measurements in China have been reviewed in brief very recently (Zhao et
99 al., 2019); 2) it is not trivial to convert measured $f(RH)$ to growth factors or κ values (Kreidenweis
100 and Asa-Awuku, 2014). Nevertheless, we note that some methods have been proposed to convert
101 measured $f(RH)$ to κ (Kuang et al., 2017; Kuang et al., 2018).

102 Single particles techniques (Krieger et al., 2012; Li et al., 2016) have provided physiochemical
103 data which are very valuable to test aerosol thermodynamic models, largely helping us better
104 understand tropospheric aerosol hygroscopicity. However, as numbers of particles examined in
105 single particle studies are very limited, these studies usually do not provide direct information of
106 overall aerosol hygroscopicity in the ambient air and thus are not discussed herein. Although not

107 covered in this review, remote sensing techniques can also be used to retrieve aerosol
108 hygroscopicity in the troposphere (Lv et al., 2017; Bedoya-Velásquez et al., 2018; Tang et al., 2019;
109 Dawson et al., 2020).

110 The first goal of this paper is to provide a comprehensive overview of hygroscopic properties
111 and CCN activities of tropospheric aerosols in China via reviewing previous field studies. The
112 second goal is to compile and present measurement data (as compiled in Tables S1-S5) reported
113 by previous work using a consistent framework (i.e. via using the single hygroscopicity parameter)
114 to enhance their accessibility and usability. The third goal, perhaps more importantly, is to identify
115 knowledge gaps in this field and then to provide an outlook which can serve as practical guidelines
116 for planning future research. In this paper, Section 2 describes the methodology adopted in this
117 paper to analyse and review previous studies, and previous measurements of hygroscopic
118 properties and CCN activities of tropospheric aerosols in China are reviewed and discussed in
119 Sections 3 and 4. In the end, Section 5 outlines knowledge gaps and research perspectives.

120 **2 Methodology**

121 **2.1 Hygroscopic properties**

122 H-TDMA instruments, initially developed ~40 years ago (Liu et al., 1978; McMurry et al.,
123 1983; Rader and McMurry, 1986; McMurry and Stolzenburg, 1989), have been widely used in
124 field and laboratory studies (Kreidenweis et al., 2005; Svenningsson et al., 2006; Gysel et al., 2007;
125 Sjogren et al., 2008; Swietlicki et al., 2008; Duplissy et al., 2009; Asmi et al., 2010; Liu et al.,
126 2011; Wu et al., 2011; Kreidenweis and Asa-Awuku, 2014; Zieger et al., 2017; Tang et al., 2019).
127 Technical details of H-TMDA measurements, including operation principles, data analysis and etc.,
128 have been detailed in a review paper (Swietlicki et al., 2008). In brief, an aerosol flow, dried to
129 <20% RH, is passed through an aerosol neutralizer and the first DMA (Differential Mobility

130 Analyzer) to produce quasi-monodisperse aerosols with a given mobility diameter; after that, the
131 aerosol flow is delivered through a humidifier to be humidified to a given RH, and subsequently
132 aerosol size distributions are measured using the second DMA coupled with a CPC (Condensation
133 Particle Counter). The hygroscopic growth factor, GF, is defined as the ratio of the aerosol mobility
134 diameter at a given RH to that at dry conditions. As aerosol particles at a given size may have
135 different hygroscopic properties and thus display different GF values at a given RH, probability
136 distribution functions of GF (i.e. number fractions of aerosol particles at each GF) have also been
137 reported in some studies.

138 The measured distribution functions of GF are usually smoothed and skewed due to several
139 reasons, e.g., the finite width of the DMA's transfer function, and several TDMA inversion
140 algorithms have been proposed to convert the H-TDMA raw data to the probability density
141 function of GF (Stolzenburg and McMurry, 1988; Stratmann et al., 1997; Voutilainen et al., 2000;
142 Cocker et al., 2001; Cubison et al., 2005; Gysel et al., 2009). The algorithm developed by Gysel
143 et al., TDMAinv, is currently the most widely used one. Errors and uncertainties of H-TDMA data
144 can come from several sources, including RH and temperature variability, electrical mobility
145 classification, particle non-equilibrium in the second DMA, and etc. Swietlicki et al. (Swietlicki
146 et al., 2008) comprehensively discussed the sources and magnitudes of these errors and how they
147 can be reduced or minimized. In addition, guidelines used for H-TDMA measurements, including
148 instrumental design, calibration, validation and operation as well as data analysis, have been
149 recommended in literature (Duplissy et al., 2009; Massling et al., 2011).

150 H-TDMA measurements of ambient aerosols were typically conducted for a few different
151 particles diameters at a given relative humidity (RH); most measurements were carried out at 90%
152 RH, though some studies also reported growth factors (GF) at other RH. To facilitate comparison

153 of GF reported at different RH, we convert GF measured at a given RH to κ using Eqs. (1-2)
154 (Petters and Kreidenweis, 2007; Tang et al., 2016):

155
$$\kappa = (GF^3 - 1)(\frac{B}{RH} - 1) \quad (1)$$

156
$$B = \exp(\frac{A}{d_0 \cdot GF}) \quad (2)$$

157 where d_0 is the dry particle diameter; A , which describes the Kelvin effects, is equal to 2.1 nm at
158 298.15 K if the surface tension is assumed to be the same as water (0.072 J m⁻²) (Petters and
159 Kreidenweis, 2007; Tang et al., 2016). Converting GF to κ also facilitates comparison between
160 hygroscopic properties and CCN activities. For a few studies which reported GF at different RH,
161 we focus GF measured at 90% RH; if the data at 90% are not available, we then choose
162 measurements at the RH closest to 90%.

163 To further facilitate comparison between different measurements, Swietlicki et al. (Swietlicki
164 et al., 2008) classified aerosol hygroscopicity into four groups according to their GF at 90% RH.
165 This methodology was adopted by Ye et al. (Ye et al., 2013) who reported aerosol hygroscopic
166 growth measurements in Shanghai. Nevertheless, Ye et al. (Ye et al., 2013) classified aerosol
167 particles into three modes (instead of four), and the criterions used are slightly different from
168 Swietlicki et al. (Swietlicki et al., 2008). Here we adopt the method proposed by Ye et al. (Ye et
169 al., 2013), who classified aerosol hygroscopicity into three modes, including the nearly-
170 hydrophobic (NH, $\kappa < 0.1$), the less-hygroscopic (LH, $0.1 < \kappa < 0.25$) and the more-hygroscopic (MH,
171 $\kappa > 0.25$) modes. However, here a few further statements are necessary. First, terminologies used
172 differ in previous studies for aerosol hygroscopicity modes. For example, bimodal aerosol
173 hygroscopicity was frequently observed in China (as discussed in Section 3), and the nearly-
174 hydrophobic mode defined by Ye et al. (Ye et al., 2013) was called the less-hygroscopic mode or

175 the low-hygroscopic mode in several studies. Second, actual aerosol hygroscopicity in the
176 troposphere may not perfectly fit into one of the three modes defined by Ye et al. (Ye et al., 2013).

177 **2.2 CCN activities**

178 A variety of instruments have been developed to measure CCN number concentrations
179 (Twomey, 1963; Sinnarwalla and Alofs, 1973; Fukuta and Saxena, 1979; Hudson, 1989; Ji et al.,
180 1998; Chuang et al., 2000; McMurry, 2000; Nenes et al., 2001; Otto et al., 2002; VanReken et al.,
181 2004; Roberts and Nenes, 2005; Frank et al., 2007; Kreidenweis and Asa-Awuku, 2014). Currently
182 the most widely used one is the continuous-flow streamwise thermal gradient CCN counter based
183 on the design of Roberts and Nenes (Roberts and Nenes, 2005; Lance et al., 2006) and
184 commercialized by Droplet Measurement Technologies, and mode details of this instrument can
185 be found elsewhere (Roberts and Nenes, 2005; Lance et al., 2006).

186 Measurements of size-resolved CCN activities have been discussed in a number of previous
187 studies (Lance et al., 2006; Frank et al., 2007; Petters et al., 2007; Rose et al., 2008; Good et al.,
188 2010; Moore et al., 2010; Rose et al., 2010; Bougiatioti et al., 2011). In many studies, an aerosol
189 flow sampled from the ambient air, after dried to <20% RH, is passed through an aerosol
190 neutralizer and then a DMA to produce quasi-monodisperse aerosols. The aerosol flow is
191 subsequently split into two flows; one flow is sampled into a CCN counter to measure number
192 concentrations of cloud condensation nuclei ([CCN]), and the other one is sampled into a CPC to
193 measure number concentrations of condensation nuclei ([CN]). At a given supersaturation,
194 activation fractions ([CCN]/[CN]) are measured as a function of particle diameter (selected using
195 the DMA) and then fitted by an activation curve to determine the activation diameter at which the
196 activation fraction is equal to 0.5 (Snider et al., 2006; Rose et al., 2008; Sullivan et al., 2009;
197 Bougiatioti et al., 2011; Cerully et al., 2011), and activation fractions can be measured at one or

198 more supersaturation as a function of particle diameter. Methods used for instrument calibration
199 and data correction, which can be found in literature (Frank et al., 2007; Petters et al., 2007; Rose
200 et al., 2008; King et al., 2009; Petters et al., 2009; Moore et al., 2010), are not discussed herein.
201 Furthermore, κ can be derived from the determined activation diameter at a given supersaturation
202 (Petters and Kreidenweis, 2007).

203 Maximum activation fractions may not approach one for ambient aerosols, and generally two
204 methods have been used to fit the data. If the maximum activation fraction of the fitted activation
205 curve is not fixed (three-parameter fit), the derived activation diameter (d_a) and single
206 hygroscopicity parameter (κ_a) describe the average properties of activated particles; if it is forced
207 to be 1 (two-parameter fit), the derived activation diameter (d_t) and single hygroscopicity
208 parameter (κ_t) describe the overall aerosol properties (Rose et al., 2010). For aerosols with bimodal
209 hygroscopicity distribution, κ_a is comparable to the κ determined using H-TDMA for the more-
210 hygroscopic mode, while κ_t is comparable to the average κ for the two modes. In addition to d_a and
211 d_t , the apparent cut-off diameter (above which [CN] is equal to [CCN] at a given supersaturation.),
212 d_{cut} (and thus κ_{cut}), can be determined if it is assumed that particles at each size are internally mixed
213 and that larger particles are activated first (Rose et al., 2010; Hung et al., 2014). The determination
214 of d_{cut} does not require size-resolved activation fractions, but needs the overall activation fractions
215 and aerosol number size distribution (Burkart et al., 2011; Hung et al., 2014). Our review paper is
216 focused on κ_a and to a less extent κ_t , and only discusses κ_{cut} when neither κ_a nor κ_t was reported.

217 In addition, [CCN] and [CCN]/[CN] were also measured at one or more supersaturation in
218 Tianjin (Deng et al., 2011; Yang et al., 2012; Zhang et al., 2012), Zhangjiakou (Hebei) (Lu and
219 Guo, 2012), Shijiazhuang (Hebei) (Lu and Guo, 2012), Xingtai (Hebei) (Wang et al., 2018b),
220 Qingdao (Li et al., 2015a), Shanghai (Leng et al., 2013; Leng et al., 2014), Guangzhou (Duan et

221 al., 2017; Duan et al., 2018) and Mt. Huang (Fang et al., 2016), as well as over marginal seas of
222 China (Zhu et al., 2019; Gao et al., 2020) and northwestern Pacific (Wang et al., 2019a; Zhu et al.,
223 2019). As these studies did not carry out size-resolved measurements and thus did not report
224 critical diameters or κ , they are not further discussed herein.

225 **3 Hygroscopic growth**

226 A number of aerosol hygroscopic growth measurements have been carried out in China since
227 2001 using H-TDMA (or very similar instruments). Most of these measurements were performed
228 in three regions with severe air pollution, including the North China Plain (NCP), Yangtze River
229 Delta (YRD) and Pearl River Delta (PRD), and these studies are discussed in Sections 3.1-3.3. In
230 addition, as discussed in Section 3.4, several measurements were also conducted at other locations
231 in the **eastern or southern** China.

232 **3.1 North China plain (NCP)**

233 The North China Plain is a heavily polluted region where many aerosol hygroscopic growth
234 measurements were conducted, and as summarized in Table S1. In this section we review the
235 measurements carried out at urban sites in Beijing (Section 3.1.1), rural sites in Beijing (Section
236 3.1.2), other urban/suburban sites (Section 3.1.3) and other rural sites (Section 3.1.4).

237 **3.1.1 Urban sites in Beijing**

238 Aerosol hygroscopic growth has been measured at three urban sites in Beijing, including the
239 PKU site, the IAP site, and the CAMS site.

240 **PKU site:** The PKU site is located on the campus of Peking University (39°59'20"N,
241 116°18'26"E), which is between the fourth and fifth ring road in the northwest of Beijing. All the
242 measurements (Massling et al., 2009; Meier et al., 2009; Wu et al., 2016; Wu et al., 2017; Wang et

243 al., 2018c) took place on the roof of a six-floor building (~30 m above ground), which is ~100 m
244 away from a major road.

245 Aerosol hygroscopic growth was first measured at the PKU site during 2004-2005 (Massling
246 et al., 2009; Meier et al., 2009). Massling et al. (Massling et al., 2009) measured aerosol
247 hygroscopic growth (at 90% RH) in June-July 2004 and January-February 2005. Aerosol
248 hygroscopicity exhibited trimodal distribution, and κ were found to be in the range of 0-0.028,
249 0.036-0.176 and 0.175-0.386 for the low-, medium- and high-hygroscopic modes (Massling et al.,
250 2009). In addition, no obvious difference in aerosol hygroscopicity was found between summer
251 and winter, because constantly high mass fractions (~50% wt) of carbonaceous materials (nearly
252 hydrophobic or less hygroscopic), related to extensive usage of fossil fuel, were observed in both
253 seasons for submicrometer particles (Massling et al., 2009). Ammonium sulfate was the major
254 inorganic species for the high-hygroscopic mode, while fresh carbonaceous materials (e.g., soot)
255 dominated the low-hygroscopic mode (Massling et al., 2009). Aerosol hygroscopicity was found
256 to increase with particle size and pollution levels (Massling et al., 2009), as more secondary
257 inorganic species were formed.

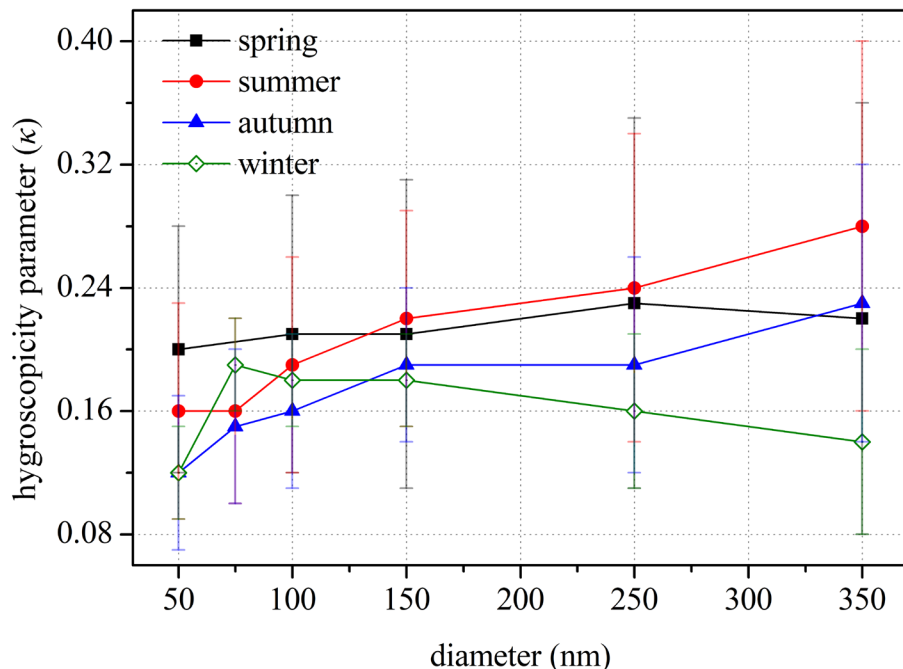
258 Meier et al. (Meier et al., 2009) further explore aerosol hygroscopic growth (at 90% RH) at
259 the PKU site in January 2005. Similar to the work by Massling et al. (Massling et al., 2009), three
260 aerosol hygroscopicity modes were identified, with the κ values being 0-0.027, 0.036-0.154 and
261 0.152-0.366 for low-, medium- and high-hygroscopic modes (Meier et al., 2009). However, no
262 obvious dependence of aerosol hygroscopicity on air pollution levels was found, as mass ratios of
263 hydrophobic species to more hygroscopic species were similar under different pollution conditions.
264 The average κ were found to first increase (30-80 nm) and then decrease with particle size (80-350
265 nm), due to increased fractions of carbonaceous species in the accumulation mode. Measured GF

266 at 90% RH were compared with these calculated from size-resolved inorganic compositions
267 measured offline, and discrepancies between measured and calculated GF were attributed to the
268 effects of organics contained (Meier et al., 2009). In addition, hygroscopic growth at 55% and 70%
269 RH was also explored for 30-400 nm aerosol particles (Meier et al., 2009), and GF at 55% and 70%
270 RH, compared to 90% RH, displayed similar dependence on particle size.

271 Wu and co-workers (Wu et al., 2016; Wu et al., 2017; Wang et al., 2018c) carried out **extensive**
272 aerosol hygroscopic growth measurements (at 90% RH) at the PKU site during 2014-2015.
273 Bimodal aerosol hygroscopicity distribution was observed in May-June 2014 (Wu et al., 2016),
274 dominated by the hydrophilic mode, and the average κ appeared to increase with particle size, from
275 0.160 at 50 nm to 0.280 at 250 nm. In addition, number fractions of aerosol particles in the
276 hydrophilic mode first increased with particle size up to 150 nm, and then did not show significant
277 change with further increase in particle size (Wu et al., 2016); to be more specific, average number
278 fractions of aerosol particles in the hydrophilic mode were ~ 0.6 at 50 nm and increased to ~ 0.8
279 above 150 nm. For each particle size, aerosol hygroscopicity was found to be larger during new
280 particle formation (NPF) periods, compared to non-NPF periods (Wu et al., 2016), because more
281 secondary species were found during NPF periods typically associated with strong photochemical
282 processes. Aerosol mass spectrometry (AMS) measurements suggested that both aerosol
283 hygroscopicity was dominated by inorganics, the contribution of which increased with particle size
284 and pollution levels (Wu et al., 2016). It was further found that the measured κ could be well
285 predicted using the AMS data, and the derived κ of organics depended linearly on their O:C ratios
286 (Wu et al., 2016).

287 The PKU site was affected by a series of biomass burning events in May-June 2014, and the
288 effect of biomass burning on aerosol composition and hygroscopicity was examined (Wu et al.,

289 2017). During biomass burning events, biomass burning contributed significantly to the production
 290 and growth of aerosols in the Aitken mode, and the contribution of organics and black carbon to
 291 mass concentrations of submicrometer aerosols reached 60% and 18% (Wu et al., 2017).
 292 Hygroscopicity and number fractions of aerosols in the hydrophobic mode were relatively
 293 invariable during biomass burning events, and the average κ , which showed no variation with
 294 particles size (50-250 nm), were determined to be ~ 0.1 (Wu et al., 2017), substantially smaller than
 295 those in the same period without significant impacts by biomass burning (Wu et al., 2016).



296
 297 **Figure 1.** Change in average κ with aerosol diameter at the PKU site in four different seasons
 298 between May 2014 to January 2015 (Wang et al., 2018c).
 299

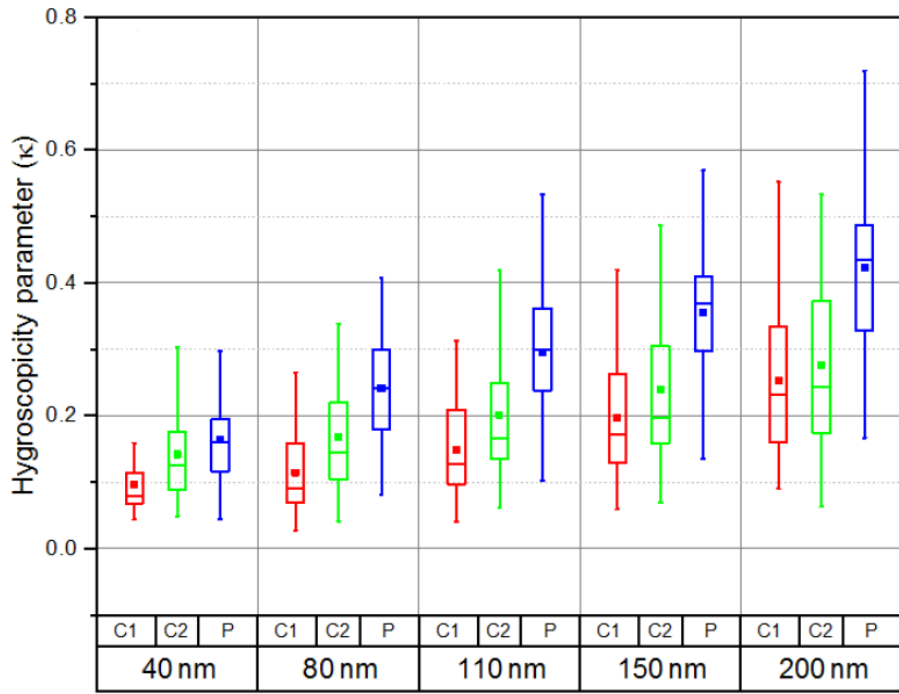
300 Seasonal variation of aerosol hygroscopic growth was investigated at the PKU site from May
 301 2014 to January 2015 (Wang et al., 2018c), and the result is displayed in Figure 1. Average κ
 302 increased significantly with particle size (50-350 nm) in summer and autumn, when strong
 303 photochemical processes enhanced secondary aerosol formation and led to particle growth (Wang

304 et al., 2018c); in fact, number fractions of particles in the hydrophilic mode increased with
305 pollution levels, and they dominated the accumulation mode when PM_{2.5} mass concentration
306 exceeded 100 $\mu\text{g}/\text{m}^3$. In contrast, as shown in Figure 1, average κ only increased slightly with
307 particles size (50-350 nm) in spring while decreased substantially with particle size (75-350 nm)
308 in winter (Wang et al., 2018c), indicating significant contribution of primary species to aerosol
309 particles. Furthermore, being different to summer and autumn, substantial amounts of aerosol
310 particles in the hydrophobic mode were always observed in spring and winter (Wang et al., 2018c).
311 Another important feature revealed by Figure 1 is that for 150-350 nm aerosols, the hygroscopicity
312 was always highest in summer and lowest in winter (Wang et al., 2018c), and the difference
313 between the two seasons increased with particle size. **The difference in aerosol hygroscopicity**
314 **between summer and winter may be caused by enhanced photochemical processes in the summer**
315 **and as a result increased fractions of secondary species.**

316 In addition, aerosol hygroscopic growth was investigated in March-April 2015 at the roof of
317 the Environmental Science Building (40°0'17"N, 116°19'34"E) on the campus of Tsinghua
318 University (Fajardo et al., 2016). This site, very close to the PKU site, is usually affected by the
319 same air masses. Number size distributions under dry and ambient conditions were measured for
320 10-500 nm particles to explore aerosol hygroscopicity under ambient RH (Fajardo et al., 2016).
321 No obvious aerosol growth was observed for RH below 50% (Fajardo et al., 2016); however, the
322 aerosol volume was increased by ~80% when RH reached 50%, and further increase in ambient
323 RH led to further hygroscopic growth.

324 **IAP site:** The IAP site is located at the Institute of Atmospheric Physics, Chinese Academy
325 of Science (39.97°N, 116.37°E) between the third and fourth ring roads in northern Beijing. All the

326 aerosol hygroscopic growth measurements (Wang et al., 2017d; Wang et al., 2019b; Fan et al.,
327 2020; Jin et al., 2020) were conducted at 90% RH at the ground level.



329 **Figure 2.** Size-resolved κ during the control clean (C1), the non-control clean (C2) and the non-
330 control polluted (P) periods. Solid squares represent the average κ , boxes represent the 25th, 50th,
331 and 75th percentiles, and extremities represent the 5th and 95th percentiles. Reprint with
332 permission by Wang et al. (Wang et al., 2017d). Copyright 2017 Copernicus Publications.

333

334 Wang et al. (Wang et al., 2017d) investigated aerosol hygroscopic growth at the IAP site in
335 August-October 2015, when emission control measures were implemented for the 2015 China
336 Victory Day parade. Three periods with different pollution levels, including the control clean (C1),
337 the non-control clean (C2) and the non-control polluted (P) periods, were specifically examined to
338 evaluate the effect of emission control. Figure 2 shows that aerosol hygroscopicity increased with
339 particle size and pollution level (Wang et al., 2017d), because mass fractions of hydrophilic species,

340 such as sulfate, nitrate and oxidized organics increased with particle size, especially under highly
341 polluted conditions. For example, κ increased from 0.100 ± 0.05 at 40 nm to 0.250 ± 0.120 at 200
342 nm during C1, from 0.140 ± 0.060 at 40 nm to 0.280 ± 0.130 at 200 nm during C2, and from
343 0.160 ± 0.080 at 40 nm to 0.420 ± 0.120 at 200 nm during the polluted period (Wang et al., 2017d).
344 Furthermore, number fractions of particles in the more hygroscopic mode increased in the polluted
345 period, compared to C1 and C2. For 40 nm particles, a quasi-unimodal hygroscopicity distribution
346 was observed during C1, while bimodal or quasi-trimodal distributions were observed during the
347 other two periods; in contrast, bimodal patterns were always observed for 150 nm particles (Wang
348 et al., 2017d). It was also found that for all the three periods, the average κ were always larger
349 during the daytime than the nighttime (Wang et al., 2017d), as aerosol particles were more aged
350 due to strong photochemical processes in daytime.

351 A following study (Wang et al., 2019b) measured aerosol hygroscopic growth at the IAP site
352 in November-December 2016. Overall the average κ were found to increase with particle size,
353 from 0.164 at 40 nm to 0.230 at 200 nm during the clean period and from 0.155 at 40 nm to 0.290
354 at 200 nm during the polluted period (Wang et al., 2019b); compared to the clean period, the
355 average κ during the polluted period were smaller for 40 nm particles but larger for 80-200 nm
356 particles. In addition, bimodal distributions were always observed (Wang et al., 2019b). Number
357 fractions of particles in the less-hygroscopic mode was larger for 40 nm particles and smaller for
358 80-200 nm particles during the polluted period (Wang et al., 2019b), when compared to the clean
359 period, reflecting the compositional variation in 40 and 80-200 nm particles during the two periods.
360 Diurnal variation of aerosol hygroscopicity was also explored, displaying significant differences
361 between clean and polluted periods (Wang et al., 2019b).

362 Jin et al. (Jin et al., 2020) further analyzed size-resolved aerosol composition and
363 hygroscopicity measured at the IAP site in November-December 2016 (Wang et al., 2019b). The
364 size-dependent κ derived from measured GF at 90% RH was used to calculate ALWC at ambient
365 RH, assuming that a constant κ could be used to calculate GF at different RH (Jin et al., 2020); in
366 addition, size-resolved aerosol composition measured using AMS was used as input in
367 ISORROPIA-II to simulate ALWC at ambient RH. ALWC simulated using ISORROPIA-II were
368 found to be significantly smaller than calculated ALWC when RH was <60% (Jin et al., 2020),
369 because ISORROPIA-II failed to estimate water uptake by organics at low RH. Overall, organic
370 materials were estimated to contribute to (30±22)% of ALWC (Jin et al., 2020), highlighting the
371 importance of organics to aerosol hygroscopicity in urban Beijing.

372 Fan et al. (Fan et al., 2020) further conducted aerosol hygroscopic growth measurements at
373 the IAP site in May-June 2017, and bimodal hygroscopicity distributions were also observed for
374 40-200 nm aerosols. The summertime measurement in 2017 was compared with the wintertime
375 measurement at the same site in 2016 (Wang et al., 2019b), and the size dependence of aerosol
376 hygroscopicity was found to differ for the two seasons (Fan et al., 2020). The average κ increased
377 from 0.158 at 40 nm to 0.271 at 110 nm in winter, and further increase in particle size (to 200 nm)
378 led to slight decrease in κ , **because mass fractions of secondary inorganic species decreased slightly**
379 **from 61.8% at 110 nm to 59.3% at 200 nm** (Fan et al., 2020). For comparison, the average κ
380 increased with particles size in summer, from 0.211 at 40 nm to 0.267 at 200 nm, **as mass fractions**
381 **of secondary inorganic species increased from 56.7% at 80 nm to 63.0% at 200 nm** (Wang et al.,
382 2019b; Fan et al., 2020). It was suggested that the size dependence of aerosol hygroscopicity was
383 mainly determined by the size-resolved mass fractions of secondary inorganic species (Fan et al.,
384 2020).

385 **CAMS site:** Wang et al. (Wang et al., 2018a) measured aerosol hygroscopic growth (30-90%
386 RH) of ambient aerosols on the campus of Chinese Academy of Meteorological Sciences, located
387 between the second and third ring roads in west Beijing. Measurements were conducted on a
388 building roof (~53 m above ground level) in December 2016, and the distance between the site
389 and a major road with heavy traffic was <200 m. Aerosol hygroscopic growth displayed unimodal
390 when RH did not exceed 60%, while bimodal distributions were usually observed at 70% and 80%
391 RH; in addition, aerosol hygroscopic growth occasionally exhibited trimodal distribution at 85%
392 and 90% RH (Wang et al., 2018a). Measured GF at 90% RH were used to calculate κ , which were
393 determined to be 0.010-0.015 and 0.286-0.358 for the hydrophobic and hydrophilic modes (Wang
394 et al., 2018a), both increasing with particle size (50-200 nm). Number fractions of hydrophobic
395 particles exceeded 50% at 50 and 100 nm, while hydrophilic particles frequently became dominant
396 in terms of number concentrations at 150 and 200 nm (Wang et al., 2018a). In addition,
397 hygroscopicity decreased at 50 nm but increased at 200 nm during heavily polluted periods (Wang
398 et al., 2018a), **when the contribution of primary emissions from local traffic to smaller particles
399 (20 and 100 nm) increased while the fractions of secondary inorganic species increased for larger
400 particles (150 and 200 nm).**

401 **3.1.2 Rural sites in Beijing**

402 Aerosol hygroscopic growth were measured at two rural sites in Beijing, including Yufa
403 (Achttert et al., 2009) and Huairou (Wang et al., 2020b). The Yufa site (39.51°N, 116.31°E) is ~1.2
404 km away from a high-traffic expressway and ~50 km south to urban Beijing, and can be considered
405 as a representative rural and regional background site. Achttert et al. (Achttert et al., 2009) measured
406 aerosol hygroscopic growth as a function of RH (56, 76, 85 and 91%) on a four-floor building (22
407 m above the ground) at this site in August-September 2006. GF at 91% RH, ranging from 1.15 to

408 1.80 for 30-300 nm particles, were found to be larger in the accumulation mode than the Aitken
409 mode (Achttert et al., 2009); furthermore, increase in mass fractions of sulfate during polluted
410 periods led to increase in aerosol hygroscopicity with pollution level. Diurnal variation of aerosol
411 hygroscopicity was also explored (Achttert et al., 2009): hygroscopicity was found to be higher in
412 the daytime than the nighttime for the Aitken mode, whereas no significant difference in
413 hygroscopicity was observed between daytime and nighttime for the accumulation mode.

414 The Huairou site (40.42°N, 116.69°E) is located on the campus of the University of the
415 Chinese Academy of Sciences, ~60 km northeast from the center of Beijing. It was mainly
416 influenced by regional transport of pollutants from downtown Beijing (Tan et al., 2018) and small
417 local sources nearly (e.g., moderate traffic and small residential areas). Aerosol hygroscopic
418 growth (at 90% RH) was measured at this site in January-March 2016 (Wang et al., 2020b). The
419 average κ were determined to be 0.162-0.208 for 50-300 nm particles (Wang et al., 2020b), and
420 mass fractions of nitrate, which contributed significantly to aerosol hygroscopic growth, reached
421 44% during polluted episodes.

422 3.1.3 Other urban/suburban sites

423 Aerosol hygroscopic growth was measured at other four urban/suburban sites in NCP,
424 including two sites in Tianjin, one site in Hebei Province and one site in Shanxi Province.

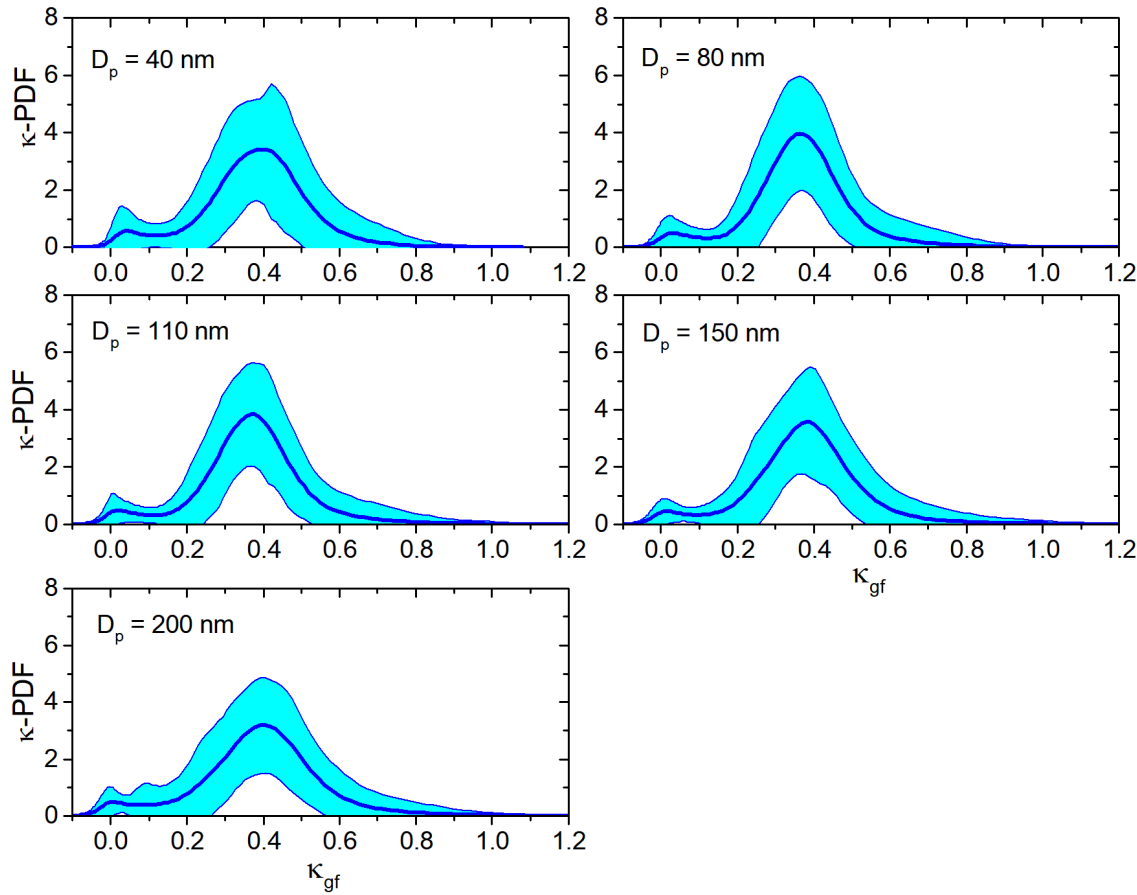
425 **Tianjin:** The Wuqing site is located next to the Wuqing Meteorological Station (39°23'N,
426 117°0'E) in the west area of Wuqing (Tianjin), surrounded by mixed agricultural, residential and
427 industrial regions. This site is a good place to study regional air pollution in NCP, as it is ~30 km
428 northwest to the urban Tianjin, ~80 km southeast to the urban Beijing, ~130 km southwest to
429 Tangshan (Hebei), and ~160 km northeast to Baoding (Hebei). Aerosol hygroscopic growth was
430 measured at three RH (90%, 95% and 98.5%) at this site in July-August 2009 (Liu et al., 2011).

431 Bimodal hygroscopicity distribution, with a dominant more-hygroscopic mode and a smaller
432 nearly-hydrophobic mode, was observed over the whole period, and the average κ , derived from
433 GF measured at 90% RH, increased from 0.250 at 50 nm to 0.340 at 250 nm, as number fractions
434 of aerosol particles in the more-hygroscopic mode increased with particle size (from 68% for 50
435 nm to 85% for 250 nm) (Liu et al., 2011). Compared to the nighttime, both the average κ and
436 number fractions of particles in the more-hygroscopic mode were larger during the daytime (Liu
437 et al., 2011), because photochemical processes during the daytime led to enhanced formation of
438 secondary species in aerosol particles and thus increase in their hygroscopicity. The average κ were
439 found to increase with particle size for the more-hygroscopic mode, from 0.310 at 50 nm to 0.390
440 at 250 nm (Liu et al., 2011); in contrast, they decreased with particle size for the nearly
441 hydrophobic mode, from 0.054 at 50 nm to 0.025 at 250 nm. It was found that secondary inorganic
442 species increased hygroscopicity of the accumulation mode while organics decreased
443 hygroscopicity of the Aitken mode (Liu et al., 2014). In addition, κ calculated from aerosol
444 compositions measured offline were consistent with those derived from H-TDMA measurements
445 (Liu et al., 2014).

446 Two different methods were used to estimate ALWC at the Wuqing site in July-August 2009
447 (Bian et al., 2014). For the first method, κ derived from GF measurements at 90-98.5% RH were
448 assumed to be constant at different RH, and thus ALWC could be calculated from particle number
449 size distribution (Bian et al., 2014); for the second method, size-resolved aerosol composition,
450 only taking into account water soluble inorganic ions, was used as input in ISORROPIA-II to
451 predict ALWC. ALWC estimated using the first method agreed with those using the second method
452 for >60% RH, but was much larger compared to the second method when ambient RH was <60%
453 (Bian et al., 2014), suggesting that ISORROPIA-II was not capable to predict ALWC at low RH.

454 In March 2018, Ding et al. (Ding et al., 2019) carried out aerosol hygroscopic growth
455 measurements (70-85% RH) at the NKU site, an air quality research supersite at Nankai University
456 (38°59'N, 117°20'E), which was ~20 km away from downtown Tianjin. GF measured at 85% RH
457 were used to calculate average κ , being 0.301-0.477, 0.203-0.386 and 0.281-0.419 on 13th, 14th
458 and 15th March (Ding et al., 2019). In addition, the average κ were found to be larger during
459 polluted periods than clean periods, as the contribution of nitrate, sulfate and ammonium in the
460 accumulation mode increased during polluted periods (Ding et al., 2019). It was also found that
461 for the accumulation mode, κ were larger in the nighttime than the daytime (Ding et al., 2019), as
462 increase in RH during the nighttime led to enhanced formation of sulfate and nitrate from aqueous
463 oxidations of SO_2 and heterogeneous hydrolysis of N_2O_5 (Wang et al., 2017a). Water-soluble
464 inorganic ions measured offline were used as input in the ISORROPIA-II to predict aerosol
465 hygroscopicity, and measured and predicted κ showed a good agreement (Ding et al., 2019),
466 implying that the contribution of organics to aerosol hygroscopic growth was quite limited.

467 **Hebei Province:** The Xingtai site is located at the National Meteorological Basic Station in
468 Xingtai (37.18°N, 114.37°E), a heavily polluted city in the center of NCP, and aerosol hygroscopic
469 growth (at 85% RH) was measured at this site in May-June 2016 (Wang et al., 2018b). As shown
470 in Figure 3, quasi-unimodal aerosol hygroscopicity distribution was observed and number
471 fractions of particles in the more-hygroscopic mode was ~90% for 40-200 nm particles (Wang et
472 al., 2018b), indicating that they were highly aged and internally mixed. As a result, the average κ
473 were found to be 0.364-0.39 (Wang et al., 2018b), significantly larger than those reported for most
474 of other sites in NCP. No obvious dependence of average κ on particle size was observed, and the
475 average κ were found to be larger in daytime than nighttime, especially during new particle
476 formation events.



477

478 **Figure 3.** Mean probability density functions of κ and their standard deviations (shaded areas) for
 479 40, 80, 110, 150 and 200 nm particles at the Xingtai site in May-June 2016, as derived from
 480 measured GF at 85% RH. Reprint with permission by Wang et al. (Wang et al., 2018b). Copyright
 481 2018 Copernicus Publication.

482

483 For the campaign at the Xingtai site in May-June 2016 (Wang et al., 2018b), aerosol
 484 hygroscopicity on a clean day (21 May) was compared with that on a highly polluted day (23 May).
 485 Aerosol hygroscopicity was higher on the polluted day (Chen et al., 2019), likely due to the
 486 enhanced formation of nitrate as revealed by ACSM (aerosol chemical speciation monitor)
 487 measurements. Furthermore, aerosol hygroscopicity increased with particles size (40-200 nm) on

488 both days, with average κ increasing from 0.288 to 0.339 on 21 May and from 0.325 to 0.352 on
489 23 May (Chen et al., 2019).

490 **Shanxi Province:** The Xinzhou site (38.24°N, 112.43°E, 1500 m above sea level) was located
491 on the border between the NCP and the Loess Plateau. This suburban and regional site, surrounded
492 by agricultural land with limited local anthropogenic emissions, was located ~360 km southwest
493 to Beijing, ~78 km northwest to Taiyuan and ~10 km south to the city nearby. Aerosol hygroscopic
494 growth (85% RH) was investigated for 25-200 nm aerosols at this site in July-August 2014 (Zhang
495 et al., 2017). Quasi-unimodal aerosol hygroscopicity distribution was observed, indicating highly
496 aged and internally mixed particles. The average κ were determined to be 0.420-0.528,
497 significantly larger than those observed at other sites in the NCP; in addition, no obvious
498 dependence of κ on particle size was found (Zhang et al., 2017). **This was because aerosols
499 observed at this site were highly aged and well internally mixed after regional transport.**

500 **3.1.4 Other rural sites**

501 Aerosol hygroscopic growth was measured at other two rural sites in NCP, i.e. the Xianghe
502 site and the Wangdu site (both in Hebei). The Xianghe site (39.75°N, 116.96°E), surrounded by
503 residential areas and farmlands, is considered as a typical rural site in NCP and is located ~5 km
504 west to the center of Xianghe town and ~70 km southeast to Beijing. At this site, aerosol
505 hygroscopic growth (at 87% RH) was measured in July-August 2013 (Zhang et al., 2016b).
506 Trimodal aerosol hygroscopicity distributions were observed for 50-350 nm particles (Zhang et al.,
507 2016b), and the average κ were determined to be 0.020-0.056, 0.170-0.211 and 0.365-0.455 for
508 nearly-hydrophobic, less-hygroscopic and more-hygroscopic modes. Aerosol hygroscopicity
509 showed some dependence on air masses (Zhang et al., 2016b): air masses which were transported
510 from the north with high speed winds typically contained larger number fractions of hydrophobic

511 species and exhibited lower hygroscopicity, whereas no obvious difference in aerosol
512 hygroscopicity and mixing state were observed for other air masses.

513 The Wangdu site (38.71°N, 115.16°E), a rural site located in the center area of NCP, was ~200
514 km southwest to Beijing, and aerosol hygroscopic growth (at 90% RH) was measured at this site
515 in June 2014 (Wang et al., 2017c). Bimodal aerosol hygroscopicity distribution was always
516 observed (Wang et al., 2017c), **indicating that aerosol particles were externally mixed. As larger**
517 **particles contain higher mass fractions of secondary inorganic species**, the average κ were found
518 to increase with particle size, from 0.240 at 30 nm to 0.320 at 250 nm.

519 **3.2 Yangtze River Delta (YRD)**

520 A number of aerosol hygroscopic growth measurements have been carried out since 2009 in
521 three large cities (Shanghai, Hangzhou and Nanjing) in the Yangtze River Delta.

522 **3.2.1 Shanghai**

523 Ambient aerosol hygroscopic growth was measured at two sites in Shanghai (Ye et al., 2011;
524 Ye et al., 2013; Wang et al., 2014; Xie et al., 2017; Li et al., 2018; Wang et al., 2020a). The FDU
525 site (31°18'N, 121°29'E) is located on the building roof of Department of Environmental Science
526 and Engineering, Fudan University; the Pudong site (31.22°N, 121.55°E) is located in Pudong
527 Meteorological Bureau. Both sites are considered as urban sites, surrounded by residential,
528 industrial and traffic areas, and their distance is <10 km.

529 **FDU site:** At the FDU site, Ye et al. (Ye et al., 2011) measured aerosol hygroscopic growth
530 (30-200 nm) at 20-85% RH in January-February 2009. Bimodal hygroscopic growth distribution
531 was always observed at 85% RH, and κ derived from measured GF at 85% RH were determined
532 to be 0.027-0.063 and 0.291-0.381 for the less- and more-hygroscopic modes (Ye et al., 2011). The
533 average κ decreased with particle size for the less hygroscopic mode while increased with particle

534 size for the more hygroscopic mode (Ye et al., 2011); in addition, number fractions of particles in
535 the less hygroscopic mode decreased with particle size. The change in GF with RH (20-85%) was
536 also discussed for particles with different sizes (Ye et al., 2011).

537 Compositional data provided by ATOFMS (Aerosol Time-of-Flight Mass Spectrometry) were
538 used to interpret GF measured at 85% RH for 250 nm particles on 18-19 January and 10 February
539 2009 (Ye et al., 2011). Bimodal aerosol hygroscopicity distribution was observed for 250 nm
540 particles, including a nearly-hydrophobic mode with κ of 0.029-0.061 and a more-hygroscopic
541 mode with κ of 0.387-0.399 (Wang et al., 2014). Aerosols in the more-hygroscopic mode consisted
542 predominantly of secondary species (e.g., OC-amine, sulfate and nitrate), while biomass burning
543 aerosols, uncoated EC, secondary organic compounds, and dust/ash were frequently identified in
544 the nearly-hydrophobic mode (Wang et al., 2014).

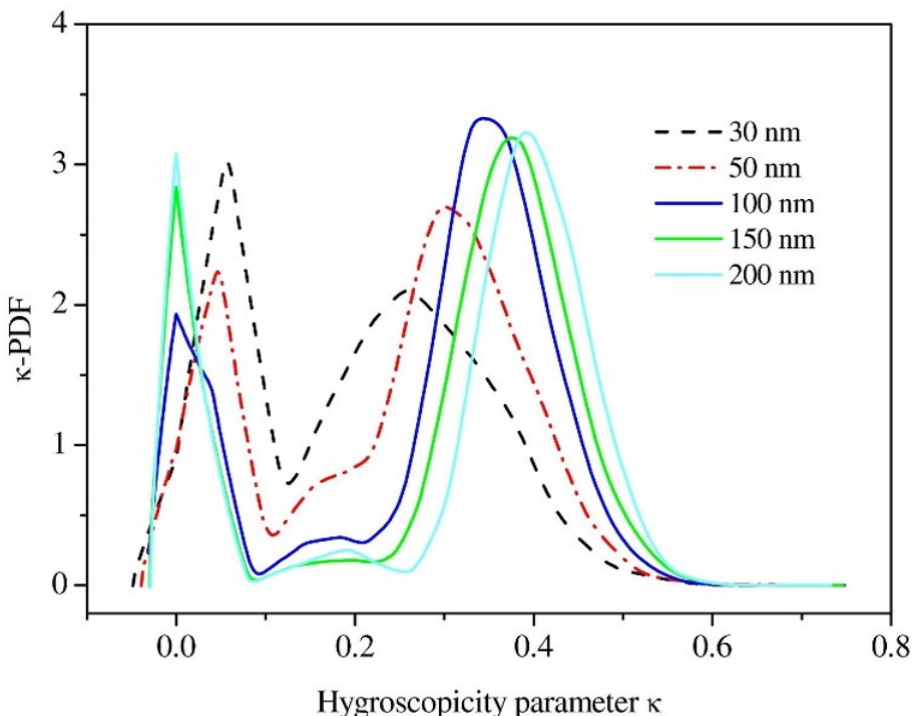
545 Aerosol hygroscopic growth (at 85% RH) was also measured at this site in February-March
546 2014 (Wang et al., 2020a). Aerosol hygroscopicity was found to exhibit bimodal distribution at
547 250 nm, and the average κ were determined to be 0.029 and 0.376 for nearly-hydrophobic and
548 more-hydrophilic modes (Wang et al., 2020a). Nearly-hydrophobic particles typically included
549 biomass burning aerosol, fresh EC and high molecular mass OC, while more-hydrophilic particles
550 included aged EC, amine-rich particles, and etc. (Wang et al., 2020a). Furthermore, a statistic
551 method was developed to estimate aerosol hygroscopicity from single particles mass spectra
552 (Wang et al., 2020a).

553 Xie et al. (Xie et al., 2017) further measured aerosol hygroscopic growth (83% RH) at the FDU
554 site in December 2014-January 2015. Bimodal aerosol hygroscopicity distribution (nearly
555 hydrophobic and more hygroscopic modes) was usually observed, and the average κ increased
556 from 0.161 at 40 nm to 0.345 at 400 nm (Xie et al., 2017). Number fractions of nearly hydrophobic

557 particles increased during polluted periods for all the sizes considered (40-400 nm), indicating
558 significant contribution of primary particles during haze events (Xie et al., 2017); however, the
559 increase in number fractions of nearly hydrophobic particles during pollution events were less
560 significant for larger particles, suggesting that primary emissions contributed more to smaller
561 particles.

562 Mixing state and hygroscopic growth (at 85% RH) were explored at the FDU site in July 2017
563 specifically for ambient black carbon (BC) aerosols (120, 240 and 260 nm) (Li et al., 2018).
564 Number fractions of BC particles decreased with particle size, from ~80% for 120 nm to ~60% for
565 360 nm. Hygroscopicity of BC particles displayed unimodal distribution, and their GF at 85% RH
566 peaked at ~1.0 (Li et al., 2018). Enhancement in hygroscopicity of BC particles, due to their aging
567 via condensation of secondary species, was frequently observed (Li et al., 2018): during the
568 nighttime nitrate contributed significantly to BC aging, while formation of secondary organic
569 materials played an important role during the daytime.

570 **Pudong site:** Aerosol hygroscopic growth (at 91% RH) was studied at the Pudong site in
571 September 2009 (Ye et al., 2013). As shown in Figure 4, aerosol hygroscopicity was found to be
572 trimodal, including a nearly-hydrophobic mode and a more-hygroscopic mode, as well as a less-
573 hygroscopic mode with much less abundance (Ye et al., 2013), implying that these aerosols were
574 externally mixed. The average κ increased from 0.270 at 30 nm to 0.390 at 200 nm for the more-
575 hygroscopic mode, because mass fractions of secondary inorganic species increased with particle
576 size (Ye et al., 2013). In contrast, the average κ decreased from 0.054 at 30 nm to 0.011 at 200 nm
577 for the nearly-hydrophobic mode.



578

579 **Figure 4.** Probability distribution functions of the hygroscopicity parameter (κ) for 30, 50, 100,
 580 150 and 200 nm aerosols at the Pudong site in September 2009. Reprint with permission by Ye et
 581 al. (Ye et al., 2013). Copyright 2013 Elsevier Ltd.

582

583 3.2.2 Hangzhou

584 Up to now only one aerosol hygroscopic growth study was carried out in Hangzhou, at the ZJU
 585 site located on the Huajiachi campus of Zhejiang University ($30^{\circ}16'N$, $120^{\circ}11'E$). Aerosol
 586 hygroscopic growth was measured at 70-90% RH (mainly at 82%) in December 2009-January
 587 2010 (Zhang et al., 2011). Bimodal hygroscopicity distribution was observed for 50-200 nm
 588 aerosols, while unimodal hygroscopicity distribution was observed for 30 nm aerosols (Zhang et
 589 al., 2011). The average κ decreased from 0.121 at 30 nm to 0.065 at 80 nm for the low-hygroscopic
 590 mode, and further increase in particle size (up to 200 nm) did not lead to significant change in κ
 591 (Zhang et al., 2011). For comparison, the average κ increased from 0.303 at 30 nm to 0.343 at 80

592 nm for the more-hygroscopic mode, and further increase in particle size only resulted in very
593 small increase in κ . In addition, number fractions of particles in the more-hygroscopic mode
594 increased from ~48% at 30 nm to ~70% at 100 nm, and remained nearly constant for 100-200 nm
595 (Zhang et al., 2011).

596 **3.2.3 Nanjing**

597 Aerosol hygroscopic growth was measured at three urban/suburban sites in Nanjing. The
598 NUIST site ($32^{\circ}20'7''N$, $118^{\circ}71'7''E$) is a suburban site located on the 12th floor of the Meteorological
599 building at Nanjing University of Information Science and Technology, with several large
600 petrochemical factories and a busy expressway nearby. The NATC site ($32.0^{\circ}N$, $118.7^{\circ}E$) is a
601 typical urban site at Nanjing Advanced Technical College, located in the centre business district
602 with heavy residential and traffic emissions. The JEMC site is an urban site on the 6th floor of the
603 building of Jiangsu Environmental Monitoring Centre (~18 m above the ground), located in the
604 urban area and surrounded by a variety of sources such as residence, restaurants, office blocks and
605 traffic.

606 **NUIST site:** Wu et al. (Wu et al., 2014) measured aerosol hygroscopic growth as a function of
607 RH (60-90%) at the NUIST site in May-July 2012, and bimodal hygroscopicity distributions were
608 frequently observed at 90% RH for 40-200 nm aerosols. For the more-hygroscopic mode, average
609 κ were determined to be 0.294-0.349, increasing with particle size (except for 40 nm); while for
610 the less-hygroscopic mode, average κ were found to decrease with particle size, from 0.079 at 40
611 nm to 0.040 at 200 nm (Wu et al., 2014). The average aerosol hygroscopicity measured at this site
612 in Nanjing seemed to be slightly lower than those reported in Beijing, Shanghai and Guangzhou.

613 Yang and co-workers further investigated aerosol (30-230 nm) hygroscopic growth (at 90%
614 RH) at this site in April-May 2014 (Xu et al., 2015; Yang et al., 2019), and bimodal hygroscopicity

615 distribution was observed. The average κ values were found to be very low (close to 0) for the low-
616 hygroscopic mode, and decreased from 0.232 at 30 nm to 0.186 at 230 nm for the medium
617 hygroscopic mode. Aerosol hygroscopicity measured in April-May 2014 (Xu et al., 2015; Yang et
618 al., 2019) were significantly lower than that measured in May-June 2012 at the same site (Wu et
619 al., 2014). One possible reason **for difference in aerosol hygroscopicity observed in the two periods**
620 **at the same site** was that in April-May 2014 organic species made a large contribution to
621 submicrometer aerosols (21-38% by mass) (Xu et al., 2015; Yang et al., 2019), thus leading to
622 substantial decrease in aerosol hygroscopicity.

623 **NATC site:** In August 2013, Li et al. (Li et al., 2015b) investigated hygroscopic growth at 90%
624 RH for 32-350 nm aerosols. A less-hydrophobic mode (κ : 0.017-0.031) and a more-hygroscopic
625 mode (κ : 0.178-0.229) were observed during the campaign (Li et al., 2015b). Aerosol
626 hygroscopicity reported at the NATC site in August 2013 (Li et al., 2015b) was lower than these
627 reported at the NUIST site in May-June 2012 (Wu et al., 2014) and in April-May 2014 (Xu et al.,
628 2015; Yang et al., 2019), perhaps because the contribution of low hygroscopic primary particles
629 (e.g., soot) from local emission was larger at the NATC site (an urban site), compared to the
630 NUIST site (a suburban site).

631 **JEMC site:** At the JEMS site, 40-200 nm aerosol hygroscopic growth was measured at 85%
632 RH in January-February 2015 (Zhang et al., 2018). The average κ were determined to be 0.200-
633 0.271 for 40-200 nm particles (Zhang et al., 2018), significantly larger than those (0.081-0.126 for
634 32-350 nm particles) reported for the NATC site in August 2013 (Li et al., 2015b), and the reason
635 was unclear. Bimodal hygroscopicity distribution was also observed (Zhang et al., 2018); similar
636 to two previous studies in Nanjing (Wu et al., 2014; Li et al., 2015b), number fractions of particles

637 in the low hygroscopic mode and their average κ both decreased with particle size, while the
638 average κ increased with particle size for the more hygroscopic mode (except for 40 nm).

639 **3.3 Pearl River Delta (PRD)**

640 A series of aerosol hygroscopic growth studies were conducted in PRD, to be more specific, at
641 two rural sites (Xinken and Wanqinsha) and one suburban site (Panyu) in Guangzhou and one
642 suburban site (HKUST) in Hong Kong.

643 **3.3.1 Rural sites in Guangzhou**

644 The Xinken site (22.6°N , 113.6°E), located near the Pearl River estuary, is ~ 50 km southeast
645 to urban Guangzhou, and the Wanqinsha site is located ~ 9 km northwest of Xinken. Both are
646 typical rural background sites with no major pollution sources nearby, and air quality at both sites
647 are affected by regional transport combined with limited local sources, such as traffic, ships,
648 biomass burning and cooking (Cheng et al., 2006; Eichler et al., 2008; Kim et al., 2011).

649 Eichler et al. (Eichler et al., 2008) measured aerosol hygroscopic growth (30-91% RH) at the
650 Xinken site in October-November 2004. The average GF at 91% RH were determined to 1.45,
651 1.53, 1.6 and 1.56 for 80, 140, 250 and 380 nm particles (Eichler et al., 2008), corresponding to κ
652 of 0.244, 0.283, 0.324 and 0.288, respectively. Inorganic aerosol compositions measured offline
653 were used to calculate GF, and the average difference between the measured and calculated GF
654 was found to be $<8\%$ (Eichler et al., 2008), suggesting that the contribution of organics to aerosol
655 hygroscopicity was rather small.

656 In a following study (Kim et al., 2011), aerosol hygroscopic growth (at 85% RH) of ultrafine
657 particles (40, 50, 60 and 80 nm) was investigated at the Wanqinsha site in October-November 2008.
658 During photochemical events, GF varied between 1.13 and 1.55, and particles consisted mainly of
659 ammonium sulfate and organic materials (Kim et al., 2011). For comparison, during combustion

660 events (i.e. affected by biomass burning and traffic emission), aerosol particles were mainly
661 composed of non-hygroscopic carbonaceous species and smaller amounts of potassium, and
662 correspondingly measured GF were reduced to 1.05-1.15 (Kim et al., 2011).

663 **3.3.2 Urban/suburban sites in Guangzhou**

664 The Panyu site, located at the top of Mt. Dazhengang (23°00'N, 113°21'E, 150 m above the sea
665 level), is surrounded by residential areas without major pollution sources nearby and can be
666 considered as a suburban site in Guangzhou (Tan et al., 2013). Several aerosol hygroscopic growth
667 measurements at 90% RH have been carried out at this site since 2011 (Tan et al., 2013; Jiang et
668 al., 2016; Cai et al., 2017; Tan et al., 2017; Cai et al., 2018; Hong et al., 2018; Liu et al., 2018a).

669 Aerosol hygroscopic growth was first measured at this site in November-December 2011 (Tan
670 et al., 2013). Bimodal hygroscopicity distributions were observed for 40, 80, 110, 150 and 200 nm
671 particles, and κ were determined to be 0.045-0.091 and 0.290-0.323 for the less- and more-
672 hygroscopic modes (Tan et al., 2013). In general, both hygroscopicity and number fractions
673 increased with particle size for the more-hygroscopic mode, whereas they both decreased with
674 particle size for the less-hygroscopic mode. Average hygroscopicity was found to be larger during
675 the daytime than the nighttime for both modes, **due to strong photochemical aging in the daytime**
676 (Tan et al., 2013), and hygroscopicity and number fractions of particles in the more-hygroscopic
677 mode increased during polluted periods, when compared to clean periods.

678 Jiang et al. (Jiang et al., 2016) compared aerosol hygroscopicity measured at this site between
679 winter (December 2012-January 2013) and summer (July-September 2013), and no obvious
680 difference in average κ was found between the two seasons. Trimodal hygroscopicity distributions
681 were observed for 40-200 nm particles, and κ were determined to be 0.290-0.339, ~0.15 and ~0.015
682 for more-, less- and non-hygroscopic modes (Jiang et al., 2016). Similar to the work by Tan et al.

683 (Tan et al., 2013), hygroscopicity and number fractions increased with particle size for the more-
684 hygroscopic mode, with no distinct difference between winter and summer (Jiang et al., 2016); for
685 the non-hygroscopic mode, hygroscopicity and number fractions both decreased with particle size,
686 and their number fractions were slightly lower in winter than in summer. The average κ were larger
687 during daytime than nighttime for both seasons, due to stronger atmospheric aging in the daytime;
688 furthermore, the diurnal variation of aerosol hygroscopicity was more profound in summer, as
689 daytime photochemical aging in the summer was more intensive than winter (Jiang et al., 2016).

690 Tan et al. (Tan et al., 2017) measured aerosol hygroscopic growth in January-March 2014, and
691 average κ increased from 0.204 at 40 nm to 0.312 at 200 nm. The κ values derived from GF
692 measured at 90% RH were used to calculate ALWC under ambient conditions, and meanwhile
693 aerosol inorganic species measured were used as input in ISORROPIA-II to predict ALWC. Good
694 agreement between calculated and predicted ALWC were found for RH >70%, but significant
695 differences were found at <70% RH (Tan et al., 2017). Liu et al. (Liu et al., 2018a) further explored
696 aerosol hygroscopic growth measured in February-March 2014 at this site, and found that the
697 average κ values increased from 0.261 at 80 nm to 0.323 at 200 nm. In addition, bimodal
698 hygroscopicity distribution was observed, and average κ increased from 0.382 at 80 nm to 0.432
699 at 200 nm for the more hygroscopic mode (Liu et al., 2018a).

700 Aerosol hygroscopic growth (at 90% RH) were further measured at this site in November-
701 December 2014 (Cai et al., 2017; Cai et al., 2018). Bimodal hygroscopicity distributions were
702 observed for 40-200 nm particles, and the average κ increased with particle size, from 0.213 at 40
703 nm to 0.312 at 200 nm. The κ values derived from size-resolved chemical compositions measured
704 using AMS were significantly lower than those derived from GF measurements (Cai et al., 2017;

705 Cai et al., 2018), probably because using a constant κ value (0.1) may underestimate
706 hygroscopicity of aerosol organics or mixed inorganic/organic aerosols.

707 Aerosol composition and hygroscopic growth at 90% RH were investigated at this site in
708 September-October 2016 (Hong et al., 2018), using an ACSM and a H-TDMA. Bimodal
709 hygroscopicity distributions were observed; the more-hygroscopic mode was dominant at 100 and
710 145 nm, while less- and more-hygroscopic modes were of similar magnitude at 30 and 60 nm
711 (Hong et al., 2018). The average aerosol hygroscopicity increased with particle size, and no
712 obvious diurnal variation was observed (Hong et al., 2018); however, aerosol hygroscopicity was
713 higher during the daytime for the less-hygroscopic mode while slightly lower in the afternoon for
714 the more-hygroscopic mode. Hygroscopicity closure analysis suggested that taking into account
715 the dependence of GF on composition for organics led to better agreement between measured and
716 calculated GF (Hong et al., 2018). It was further found that GF increased linearly with O:C ratios
717 for organics, and the derived GF appeared to be less sensitive to the changes of O:C ratios during
718 polluted periods.

719 **3.3.3 Hong Kong**

720 Since 2011, H-TDMA and online mass spectrometry were employed by Chan and co-workers
721 (Lopez-Yglesias et al., 2014; Yeung et al., 2014; Cheung et al., 2015) to investigate aerosol
722 composition and hygroscopic growth at the HKUST supersite (22°20'N, 114°16'E) on the east coast
723 of Hong Kong. It is a typical suburban and coastal site with no major pollution sources nearby.

724 Aerosol hygroscopic growth at 90% RH was first investigated at this site in 2011 (Yeung et al.,
725 2014), and bimodal aerosol hygroscopicity distributions were observed with a dominant more-
726 hygroscopic mode and a weak less-hygroscopic mode at 75, 100, 150 and 200 nm. The average κ
727 were determined to be 0.330-0.360 during May, 0.370-0.390 during the first half of September,

728 0.210-0.250 during the second half of September and 0.290-0.320 during November (Yeung et al.,
729 2014), caused by compositional variations in different air masses. **Since aerosol particles arriving**
730 **at this site were heavily aged and well internally mixed**, no obvious dependence of average κ on
731 particle size was found.

732 Number fractions of particles in the more-hygroscopic mode were always >0.8 (Yeung et al.,
733 2014), except for 75 nm particles in the second half of September (~ 0.45) which was dominantly
734 affected by continental air masses. When compared to maritime aerosols, hygroscopicity of
735 aerosols in the more-hygroscopic mode was substantially lower for continental aerosols which
736 contained larger proportions of organic **matters** (Yeung et al., 2014). Hygroscopicity closure
737 analysis suggested that using a constant GF (1.18) at 90% RH for organic materials, instead of
738 considering the dependence of GF on their oxidation degree, would lead to better agreement
739 between measured and calculated GF (Yeung et al., 2014), likely because inorganic species (such
740 as sulfate) contributed dominantly to the overall aerosol hygroscopicity during the entire campaign.

741 In addition, hygroscopic growth at the HKUST site was investigated as a function of RH (10-
742 90%) in 2011-2012 (Lopez-Yglesias et al., 2014; Cheung et al., 2015), and both hysteresis behavior
743 and continuous hygroscopic growth of ambient aerosols were observed.

744 **3.4 Other locations**

745 In addition to NCP, YRD and PRD, measurements of aerosol hygroscopic growth were also
746 conducted in other regions in China, as discussed below.

747 **Taipei:** Hygroscopic growth (15-90% RH) was investigated for 53, 82, 95 and 202 nm aerosols
748 at an urban site in Taipei (Taiwan Province) in October-December 2001 (Chen et al., 2003).
749 Bimodal hygroscopicity distribution was observed for all the particles at 90% RH: while κ (0.049-
750 0.068) showed no obvious dependence on particle size for the less hygroscopic mode, they

751 increased from 0.274 at 53 nm to 0.422 at 202 nm for the more hygroscopic mode (Chen et al.,
752 2003). No obvious hygroscopic growth was observed at <45% RH (Chen et al., 2003), and bimodal
753 hygroscopic growth behavior appeared at ~76% RH for all the sizes (53-202 nm), becoming more
754 noticeable with further increase in RH.

755 **Mt. Huang:** Mt. Huang (30°08'N, 118°09'E) is located in the mountainous area of east China
756 with large forest coverages and limited anthropogenic activities. Aerosol hygroscopic growth at
757 50-85% RH was examined in September-October 2012 at the mountain foot (~464 m above the
758 sea level) and the mountain top (~1860 m above the sea level) (Wu et al., 2018a). No significant
759 particle growth was observed below 60% RH at both sites, and bimodal growth behavior appeared
760 at ~75% RH except 40 nm particles and became more evident at higher RH (**80% and 85%**) (Wu
761 et al., 2018a). Hygroscopicity was higher in the daytime than the nighttime for both modes. In
762 addition, hygroscopicity was slightly higher at the mountain foot than the mountain top for both
763 modes (except 200 nm particles in the more-hygroscopic mode) (Wu et al., 2018a); the reason was
764 that more secondary inorganic species were formed at the mountain foot due to human activities,
765 while on the mountain top the contribution of organics increased. Compared to NCP, YRD and
766 PRD sites, the overall aerosol hygroscopicity was lower at Mt. Huang (Wu et al., 2018a), as it is
767 located in a clean region with smaller fractions of secondary inorganic aerosols.

768 In July 2014 aerosol hygroscopic growth (at 85% RH) was further studied at the top of Mt.
769 Huang (Xu, 2015; Chen et al., 2016; Wang et al., 2016). The average κ were determined to be
770 0.275, 0.266 and 0.290 at 70, 150 and 230 nm (Chen et al., 2016; Wang et al., 2016), in good
771 agreement with the previous study conducted at the same site in 2012 (Wu et al., 2018a). At a
772 given particle size, aerosol hygroscopicity was found to be higher in the daytime than the nighttime
773 (Chen et al., 2016; Wang et al., 2016); furthermore, aerosol hygroscopicity was higher for air

774 masses from northwest than those from southeast. The derived κ depended positively on mass
775 fractions of inorganics and negatively on organics (Chen et al., 2016; Wang et al., 2016). In
776 addition, unimodal aerosol hygroscopicity distribution occurred with high frequency (47.5%)
777 during the campaign, and it also appeared more frequently in the afternoon with GF (at 85% RH)
778 in the range of 1.25-1.45 (Chen et al., 2016; Wang et al., 2016).

779 **Shouxian:** In June-July 2016, Qian et al. (Qian et al., 2017) studied hygroscopic growth (at
780 90% RH) of 50-250 nm aerosols at Shouxian National Climate Observatory (32°26'N, 116°48'E)
781 in east China, a rural site surrounded by farmlands at Shouxian, Anhui Province. Bimodal aerosol
782 hygroscopicity distribution was observed, and the average κ increased with particle size, from
783 0.129 at 50 nm to 0.279 at 250 nm (Qian et al., 2017).

784 **East China Sea:** Total suspended particles were collected during a cruise over the East China
785 Sea (22-35°N and 119-126°E) in May-June 2014 and dissolved in deionized water. The resulting
786 solutions were atomized to generated aerosols, and their hygroscopic growth was then measured
787 at 5-90% RH (Yan et al., 2017). The average κ was determined to be 0.88 for the whole cruise, and
788 the daytime average (0.81) was smaller than the nighttime average (0.95) (Yan et al., 2017), due
789 to less chloride loss in the nighttime. It is to be assessed to which extent aerosols generated by Yan
790 et al. (Yan et al., 2017) can actually mimic ambient aerosols.

791 **3.5 Summary**

792 Geographically speaking, almost all **of** the aerosol hygroscopic growth studies were conducted
793 in east China, especially in NCP, YRD and PRD. Aerosol hygroscopic growth in other regions in
794 China remains to be explored, and measurements at rural and remote areas with limited
795 anthropogenic impacts are very scarce. In addition, previous measurements were mainly

796 performed at or close to the ground level, except these carried out on the top of Mt. Huang (Chen
797 et al., 2016; Wang et al., 2016; Wu et al., 2018a).

798 It can be concluded that submicrometer aerosols in China usually exhibit bimodal
799 hygroscopicity distribution (i.e. nearly-hydrophobic and more-hygrosopic modes). Trimodal
800 distributions, with a medium-hygrosopic mode with limited importance, were also reported by
801 several studies (Massling et al., 2009; Meier et al., 2009; Ye et al., 2013; Jiang et al., 2016; Zhang
802 et al., 2016b; Wang et al., 2017d; Wang et al., 2018a). **Bimodal or trimodal hygroscopicity**
803 **distributions suggested that aerosol particles under investigation were externally mixed.** Quasi-
804 unimodal hygroscopicity distributions existed but were quite sparse (Chen et al., 2016; Wang et
805 al., 2016; Wang et al., 2017d; Zhang et al., 2017; Wang et al., 2018b), **implying that these aerosols**
806 **were nearly internally mixed.**

807 For the more-hygrosopic mode, κ usually increased with particle size, except for the
808 measurements carried out at HKUST site (Yeung et al., 2014) where no obvious dependence on
809 particle diameter was found. For the nearly-hydrophobic mode, κ usually decreased with particle
810 size (Liu et al., 2011; Ye et al., 2011; Zhang et al., 2011; Tan et al., 2013; Ye et al., 2013; Wu et al.,
811 2014; Jiang et al., 2016; Zhang et al., 2016b; Qian et al., 2017; Zhang et al., 2018), though **opposite**
812 results were also reported in several studies (Chen et al., 2003; Massling et al., 2009; Meier et al.,
813 2009; Li et al., 2015b; Wang et al., 2018a; Wu et al., 2018a).

814 Average aerosol hygroscopicity, especially for the more-hygrosopic mode, usually increased
815 with pollution levels (Massling et al., 2009; Wu et al., 2016; Wang et al., 2017d; Wang et al., 2018a;
816 Chen et al., 2019; Ding et al., 2019; Wang et al., 2019b), attributed to increased mass fractions of
817 secondary inorganic aerosols. However, different results were also reported, especially for particles

818 at or below 50 nm (Achert et al., 2009; Meier et al., 2009; Wang et al., 2018a; Wang et al., 2019b)
819 for which primary emissions could play an important role.

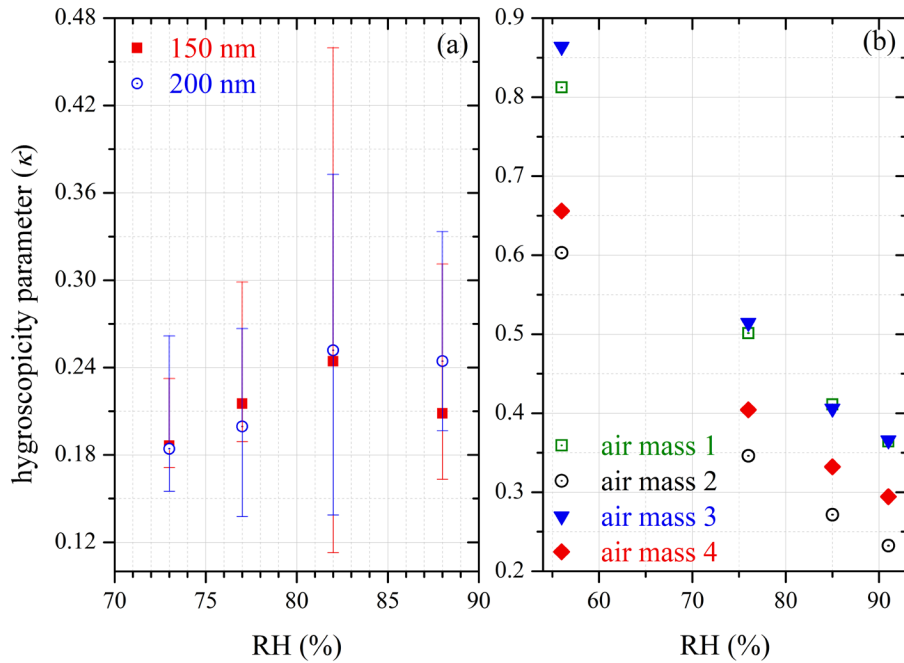
820 A few studies examined aerosol hygroscopic growth at different seasons (Massling et al., 2009;
821 Jiang et al., 2016; Wang et al., 2018c; Fan et al., 2020). No obvious difference in the overall aerosol
822 hygroscopicity was observed between summer and winter at the PKU site (Beijing) (Massling et
823 al., 2009), the IAP site (Beijing) (Fan et al., 2020) and the Panyu site (Guangzhou) (Jiang et al.,
824 2016). However, one study (Wang et al., 2018c) suggested that the overall hygroscopicity, and
825 especially hygroscopicity of 150-350 particles, was highest in summer and lowest in winter at the
826 PKU site (Beijing); one possible reason was that aerosol particles examined by Wang et al. (2018c)
827 were most aged in the summer (and thus contained largest fractions of secondary species with high
828 hygroscopicity) and least aged in the winter.

829 Diurnal variations of aerosol hygroscopic growth were also investigated. Most of these studies
830 suggested that aerosol hygroscopicity was generally higher in the daytime, compared to the
831 nighttime. For example, hygroscopicity was higher in the daytime than the nighttime for the Aitken
832 mode at the Yufa site (Beijing) in August-September 2006 (Achert et al., 2009), while no
833 significant difference was found between daytime and nighttime for the accumulation mode. In
834 addition, aerosol hygroscopicity was found to be higher at the daytime than the nighttime at the
835 IAP site (Beijing) in August-October 2015 (Wang et al., 2017d), at the Wuqing site (Tianjin) in
836 July-August 2009 for the more hygroscopic mode (Liu et al., 2011), at the Xingtai site (Hebei) in
837 May-June 2016 (Wang et al., 2018b), at the Panyu site (Guangzhou) in November-December 2011
838 (Tan et al., 2013), December 2012-January 2013 (Jiang et al., 2016) and July-September 2013
839 (Jiang et al., 2016), and at Mt. Huang in September-October 2012 (Wu et al., 2018a) and July 2014
840 (Chen et al., 2016; Wang et al., 2016). The underlying reason was that photochemical processes

841 during the daytime led to increased relative contribution of secondary aerosols, which were very
842 hygroscopic. However, there are also exceptions. For example, κ was larger in the nighttime than
843 the daytime for the accumulation mode at the NKU site (Tianjin) in March 2017 (Ding et al., 2019),
844 as high RH in the nighttime may enhance sulfate and nitrate formation from aqueous oxidation of
845 SO₂ and heterogeneous hydrolysis of N₂O₅ (Wang et al., 2017a). In addition, no obvious diurnal
846 variation in average aerosol hygroscopicity was observed at the Panyu site (Guangzhou) in
847 September-October 2016 (Hong et al., 2018), though aerosol hygroscopicity was higher during the
848 daytime for the less hygroscopic mode and slightly lower in the afternoon for the more-
849 hygroscopic mode.

850 While aerosol hygroscopic growth measurements were typically carried out at a single RH at
851 around 90%, several studies also investigated aerosol hygroscopic growth as different RH (Chen
852 et al., 2003; Eichler et al., 2008; Achtert et al., 2009; Meier et al., 2009; Liu et al., 2011; Ye et al.,
853 2011; Zhang et al., 2011; Cheung et al., 2015; Wang et al., 2018a; Wu et al., 2018a). As shown in
854 Figure 5, for the measurement carried out at ZJU site (Hangzhou) in December 2009-January 2010
855 (Zhang et al., 2011), average κ derived from measured GF at different RH (73-88%) varied from
856 0.186 to 0.244 for 150 nm particles and from 0.184 to 0.252 for 200 nm particles. For the
857 measurement carried out at the Yufa site (Beijing) in August-September 2006 (Achtert et al., 2009),
858 average κ were found to decrease with increasing RH (56-91%) for 250 nm particles, varying from
859 ~0.3 to ~0.8. Considerable variations of κ with RH were also reported in other studies (Chen et al.,
860 2003; Meier et al., 2009; Ye et al., 2011; Cheung et al., 2015). Therefore, it can be concluded that
861 using a constant κ to describe aerosol hygroscopic growth at different RH may not always be proper.
862 In addition, during most H-TDMA measurements aerosols were first dried at low RH (typically
863 <15%) and then humidified to a given RH, and as a result these measurements could not simulate

864 the formation of supersaturated droplets which may exist even when RH was below the
865 corresponding deliquescence RH but above the efflorescence RH.



866

867 **Figure 5.** Single hygroscopicity parameters (κ) derived from GF measured as different RH. (a)
868 150 and 200 nm particles at the ZJU site (Hangzhou) in December 2009-January 2010 (Zhang et
869 al., 2011); (b) 250 nm particles at the Yufa site (Beijing) in August-September 2006 for four typical
870 air masses (Achttert et al., 2009). Error bars are not shown in Figure 5b as uncertainties are not
871 provided in the original paper.

872

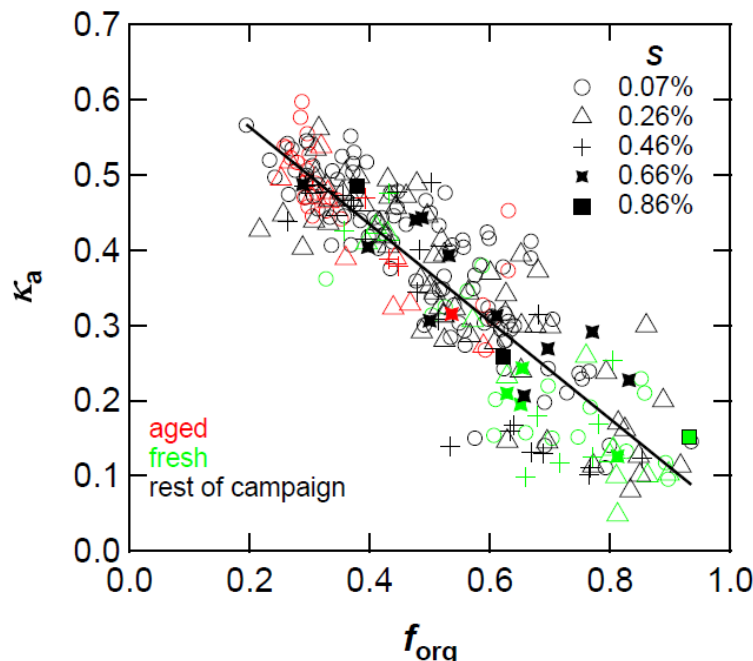
873 4 CCN activities

874 As stated in Section 2.2, we only discuss CCN activity measurements which reported κ values
875 herein. Sections 4.1-4.3 review measurements conducted in NCP, YRD and PRD, and
876 measurements carried out in other regions in China are discussed in Section 4.4.

877 **4.1 North China plain (NCP)**

878 **4.1.1 Beijing**

879 In August-September 2006, size-resolved CCN activities were measured at the Yufa site
880 (Gunthe et al., 2011). Maximum activation fractions were around 1 for supersaturation in the range
881 of 0.26-0.86%; however, they only reached ~0.8 on average at 0.07% supersaturation, and these
882 inactive particles were mainly soot. For the entire measurement period, the average κ_a and κ_t were
883 both determined to be 0.3 ± 0.1 . CCN activities were found to increase with particle size due to
884 increased mass fractions of soluble inorganics (Gunthe et al., 2011), and κ_a was measured to be
885 ~0.2 at ~40 nm and ~0.5 at 200 nm. During periods affected by aged regional pollution, mass
886 fractions of soluble inorganics were enhanced, leading to increase in κ_a (0.35 ± 0.05) (Gunthe et al.,
887 2011); in contrast, mass fractions of organics increased during periods influenced by fresh city
888 pollution, resulting in decrease in κ_a (0.22 ± 0.07).



889

890 **Figure 6.** Dependence of κ_a on mass fractions of organics for three periods over the campaign (red:
891 the aged regional pollution period; green: the fresh city pollution period; black: the rest of the

892 campaign). Reprint with permission by Gunthe et al. (Gunthe et al., 2011). Copyright 2011
893 Copernicus Publications.

894
895 As shown in Figure 6, the measured CCN activities decreased as mass fractions of organics
896 increased (Gunthe et al., 2011); furthermore, the measured κ_a could be quantitatively described by
897 mass fractions of soluble inorganics and organics, and their κ were determined to be 0.7 and 0.1.
898 Aerosol CCN activities during a rapid particle growth event on 23 August were further examined
899 (Wiedensohler et al., 2009), during which CCN size distribution was dominated by the growing
900 nucleation mode instead of the accumulation mode in usual.

901 Measurements were carried out at the PKU site to investigate size-resolved CCN activities in
902 May-June 2014 (Wu et al., 2017). Similar to the concurrent H-TDMA measurements, average κ_a
903 was determined to be ~ 0.10 during biomass burning events, displaying no dependence on particles
904 size (Wu et al., 2017). CCN activities of submicrometer particles were significantly reduced during
905 biomass burning periods, due to increased mass fractions of organics and black carbon.
906 Furthermore, average κ calculated from aerosol compositions measured using AMS were
907 consistent with those derived from hygroscopic growth and CCN activity measurements (Wu et
908 al., 2017), if κ were assumed to be **0.53 for inorganics and 0 for organics, respectively.**

909 Zhang et al. (Zhang et al., 2017) investigated size-resolved CCN activities at the IAP site in
910 November-December 2014 and August-September 2015, and maximum activation fractions were
911 found to be much smaller than one, indicating large fractions of CCN-inactive particles from local
912 primary emissions. The average κ_a , which ranged from 0.22 to 0.31 for 60-150 nm particles and
913 increased with particle size (Zhang et al., 2017), agreed well with those derived from the
914 concurrent H-TDMA measurements (Wang et al., 2017d). In addition, κ (0.32 ± 0.11) calculated

915 using ACSM-measured aerosol composition were significantly larger than those derived from
916 hygroscopic growth (0.25 ± 0.08) and CCN activities (0.26 ± 0.04) (Zhang et al., 2017). This was
917 because hygroscopicity estimated using ACSM-measured composition did not consider the
918 contribution of smaller and less-hygroscopic particles (aerosol hygroscopicity **was** lower for
919 smaller particles, but ACSM only detected >60 nm particles). **In addition, the uncertainties**
920 **associated with κ values assumed for ammonium sulfate, ammonium nitrates and organics may**
921 **also contribute to the discrepancies between measurement and calculation.**

922 In November-December 2016, Zhang et al. (Zhang et al., 2019a) further investigated size-
923 resolved CCN activities at the IAP site and found that [CCN] was significantly increased during
924 nucleation-initiated haze episodes. It was suggested that increase in particle size contributed $>80\%$
925 to the observed increase in [CCN] (Ren et al., 2018; Zhang et al., 2019a), while the effect of aerosol
926 hygroscopicity enhancement, due to change in aerosol composition, was much smaller.

927 **4.1.2 Other locations in NCP**

928 Zhang et al. (Zhang et al., 2014; Zhang et al., 2017) measured size-resolved CCN activities at
929 the Xianghe site (39.75°N , 116.96°E) in June-July 2013. Average κ_a were determined to be 0.24 -
930 0.32 during polluted periods, showing no dependence on particle size; in contrast, κ_a increased
931 from ~0.22 at ~50 nm to ~0.38 at ~180 nm for background days (Zhang et al., 2014). Compared
932 to polluted periods, κ_a were $\sim20\%$ larger under background conditions for the accumulation mode
933 (100 - 200 nm), as the contribution of aerosol organics from fresh biomass burning was significantly
934 increased during pollution events (Zhang et al., 2014); however, κ_a were very similar for the
935 nucleation/Aitken modes (40 - 100 nm) under background and polluted conditions.

936 Size-resolved CCN activities were further investigated at Xianghe site in July-August 2013
937 (Ma et al., 2016; Tao et al., 2020), and it was found that κ_a increased with particle size, from

938 0.22±0.02 at 46 nm to 0.38±0.02 at 179 nm. Compared to κ values (increasing from 0.291±0.089
939 at 50 nm to 0.373±0.092 at 350 nm) derived from concurrent H-TDMA measurements, aerosol
940 hygroscopicity derived from CCN activities were slightly lower for <50 nm particles but higher
941 for >100 nm particles (Ma et al., 2016; Zhang et al., 2016b), but the differences were quite small.

942 Zhang and co-workers (Zhang et al., 2016a; Li et al., 2017b; Zhang et al., 2017) also
943 investigated size-resolved CCN activities at the Xinzhou site in July-August 2014. The average κ_a
944 were determined to be 0.42-0.51 for 37-150 nm particles, exhibiting no dependence on particle
945 size (Zhang et al., 2017); in addition, compared to other sites in the NCP, aerosols at the Xinzhou
946 site displayed significantly higher CCN activities. This is because aerosols observed at this site
947 were highly aged and well internally mixed after undergoing regional transport for a long time,
948 and thus the variation of chemical compositions with particle size was negligible. The average κ_a
949 (0.48±0.07) (Zhang et al., 2017) agreed well with that (0.47±0.03) determined from concurrent H-
950 TDMA measurements (Zhang et al., 2017), both much significantly larger than that (0.41±0.06)
951 calculated from ACSM-measured aerosol composition, probably because such calculation may
952 underestimate the hygroscopicity of aerosol organics.

953 4.2 Yangtze River Delta (YRD)

954 Size-resolved CCN activity measurements were conducted in August 2013 at the NBM site
955 (32.04°N. 118.70°E) on the Jiangxi Island in the Yangtze River (Ma et al., 2017). This site, located
956 in a suburban area of Nanjing, did not have significant local emission at that time. The κ_a values
957 were found to range from ~0.1 to ~0.8 during the campaign, being 0.35±0.13 on average (Ma et
958 al., 2017), and no significant variation in average κ_a was found for biomass burning, urban, marine
959 and industrial air masses. In addition, κ_a increased from 0.30±0.08 at ~55 nm to 0.34±0.08 at 67
960 nm, due to larger contribution of low-hygroscopic organics at 50 nm; however, further increase in

961 particle size up to \sim 149 nm did not lead to obvious increase in κ_a (Ma et al., 2017), likely because
962 aerosols arriving at this site were heavily aged and well internally mixed.

963 Long-term size-resolved CCN activities were studied in January-December 2013 at the Lin'an
964 site (Hangzhou, Zhejiang Province) (Che et al., 2016; Che et al., 2017), which is a WMO Global
965 Atmospheric Watch regional station (30.3°N, 119.73°E, 138 m above the sea level) located in the
966 center of YRD. Maximum activation fractions were close to one at high supersaturation but only
967 reached \sim 0.89 at 0.1% supersaturation. Values of κ_a and κ_t were almost identical (\sim 0.25) at 40-50
968 nm and increased to \sim 0.42 (κ_a) and \sim 0.40 (κ_t) at 100-150 nm (Che et al., 2017), suggesting that
969 larger particles contained larger fractions of hygroscopic species (e.g., soluble inorganics).
970 Furthermore, CCN activities were also compared under nine different weather-pollution conditions
971 (Che et al., 2016), and κ were determined to be \sim 0.7 and \sim 0.1 for inorganics and organics during
972 haze episodes and \sim 0.6 and \sim 0.2 for other episodes.

973 **4.3 Pearl River Delta (PRD)**

974 Rose et al. (Rose et al., 2010; Rose et al., 2011) explored size-resolved CCN activities in July
975 2006 at the Backgarden site, which is a suburban site (23.55°N, 113.07°E) located \sim 60 km
976 northwest of Guangzhou. Maximum activation fractions were close to 1 at medium and high
977 supersaturation (0.47-1.27%) and well below 1 at low supersaturation (0.068-0.27%) (Rose et al.,
978 2010), and particles not activated were mainly externally mixed soot with an estimated median κ
979 of \sim 0.01 (Rose et al., 2011). The average κ_a and κ_t were determined to be 0.34 and 0.30 over the
980 entire campaign; to be more specific, κ_a and κ_t were almost identical (\sim 0.3) for small particles and
981 increased to 0.4-0.5 and \sim 0.33 for large particles (Rose et al., 2010). Increase in average κ_a with
982 diameter was mainly due to enhanced mass fractions of inorganics for larger particles (Rose et al.,
983 2011). Compared to the rest of the campaign, κ_a and κ_t were reduced by \sim 30% on average during

984 biomass burning events (0.34 versus 0.24), when mass fractions of organics were substantially
985 increased; moreover, the decrease in κ_t during biomass burning events was very substantial for
986 <100 nm particles but quite small for ~ 200 nm particles (Rose et al., 2010). It was further found
987 that assuming κ to be ~ 0.6 for inorganics and ~ 0.1 for organics could approximate the observed
988 CCN activities over the entire campaign (Rose et al., 2011).

989 Size-resolved CCN activities were investigated at the Panyu site in November-December 2014
990 (Cai et al., 2018), and the average κ_a were found to increase from 0.21 at 58 nm to 0.30 at 156 nm,
991 because mass fractions of organics, measured using AMS, decreased with particle size. The
992 average κ derived from H-TDMA measurements agreed well with those derived from CCN
993 measurements; however, they were larger than those calculated from size-resolved chemical
994 compositions, and the difference between measured and calculated κ increased with particle size
995 (Cai et al., 2018). This discrepancy was probably because assuming a constant κ (0.1) may
996 underestimate the hygroscopicity of aerosol organics.

997 Aerosol CCN properties were studied at the HKUST site in May 2011 (Meng et al., 2014), and
998 maximum activation fractions were found to exceed 0.9 for the entire campaign, implying that the
999 difference between κ_a and κ_t should be small. CCN activities were found to increase with particle
1000 size, with average κ_a being determined to be 0.28 at 46 nm to 0.39 at 116 nm (Meng et al., 2014),
1001 due to increase in volume fractions of inorganics as revealed by AMS measurements. It was further
1002 found that the measured κ_a could be reasonably well predicted using volume fractions of inorganics
1003 and organics (Meng et al., 2014), and their κ were determined to be 0.6 and 0.1.

1004 **4.4 Other locations**

1005 Hung et al. (Hung et al., 2014; Hung et al., 2016) measured [CCN], [CN] and aerosol number
1006 size distribution in August 2011 at a rural site and in June 2012 at an urban site in Taiwan. The

1007 rural site (25.89°N, 121.57°E) is ~15 km away from Taipei, while the urban site (25.01°N, 121.54°E)
1008 is located on the campus of National Taiwan University in a metropolitan area of Taipei. At the
1009 rural site, κ_{cut} increased from ~0.1 at ~50 nm to ~0.35 at ~165 nm during the first period which
1010 was significantly affected by anthropogenic emissions, while increased from ~0.04 at ~70 nm to
1011 ~0.28 at ~175 nm for the second period not significantly affected by anthropogenic emissions
1012 (Hung et al., 2014). Overall, κ_{cut} was larger in the first period than the second period, probably due
1013 to the impacts of aged air masses originating from cities nearby during the first period. Compared
1014 to the rural site, κ_{cut} were much smaller at the urban site, increasing from ~0.021 at ~90 nm to 0.10
1015 at ~250 nm (Hung et al., 2016), indicating that fresh anthropogenic aerosols tended to exhibit lower
1016 hygroscopicity.

1017 Shipborne size-resolved CCN activity measurements were carried out in September 2012 over
1018 remote regions of the South China Sea and East China Sea (Atwood et al., 2017). Under marine
1019 background conditions, the average κ_a were determined to be 0.65 ± 0.11 and 0.46 ± 0.17 for the
1020 accumulation and Aitken modes (Atwood et al., 2017). Compared to marine background
1021 conditions, CCN activities were reduced after extensive precipitation, with average κ_a determined
1022 to be 0.54 ± 0.14 and 0.34 ± 0.11 for the accumulation and Aitken modes; whereas during periods
1023 impacted by biomass burning, κ_a was reduced to 0.40 ± 0.03 for the accumulation mode but
1024 increased instead to 0.56 ± 0.25 for the Aitken mode (Atwood et al., 2017).

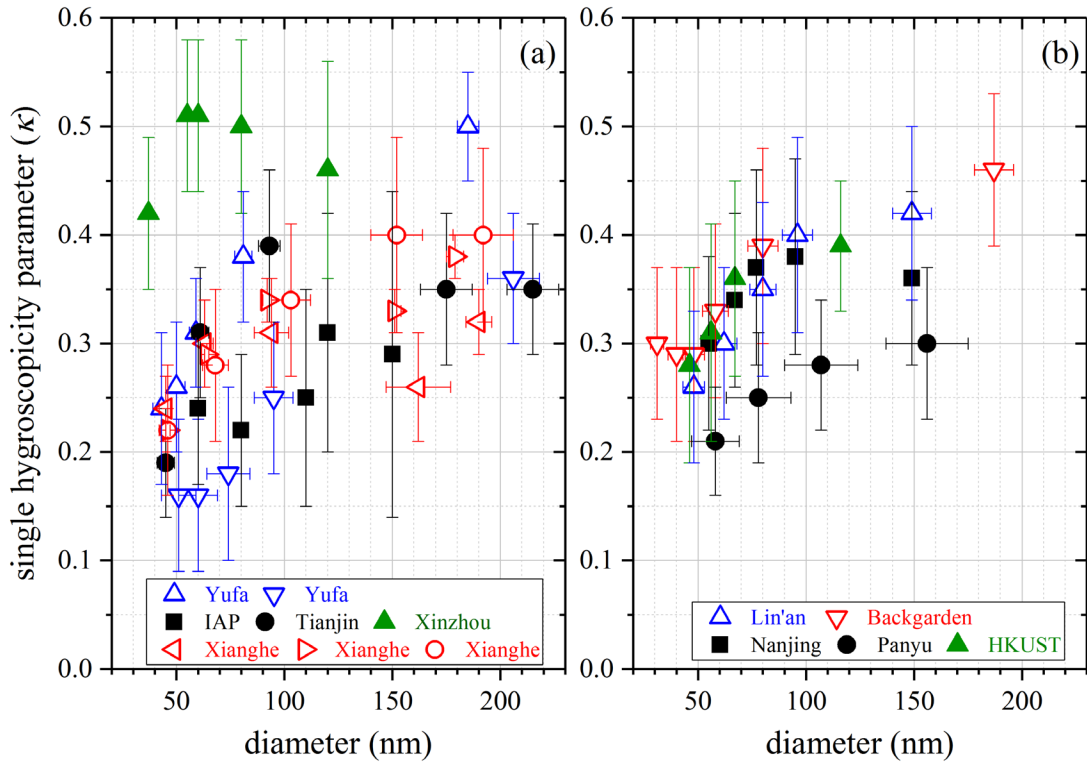
1025 Size-resolved CCN activities were explored over north South China Sea ($19^{\circ}39'N$ to $22^{\circ}43'N$,
1026 $113^{\circ}44'E$ to $118^{\circ}12'E$) in August 2018 (Cai et al., 2020), and no obvious dependence of κ_a on
1027 particle size (50-100 nm) was observed. The campaign-averaged κ was determined to be ~0.40
1028 (Cai et al., 2020), larger than these measured in the PRD region but smaller than those measured

1029 over remote marine regions. This is because the air in north South China Sea was affected by both
1030 continental air masses (low hygroscopicity) and marine background (high hygroscopicity).

1031 **4.5 Summary**

1032 Similar to H-TDMA measurements, CCN activity measurements in China were mainly carried
1033 out in NCP, YRD and PRD, and almost all the measurements took place at or close to the ground
1034 level. In addition, the number of CCN activity measurements is much smaller than H-TDMA
1035 measurements. The limited number of field studies preclude any solid conclusions on diurnal and
1036 seasonal variations of aerosol CCN activities being drawn.

1037 Maximum activation fractions were typically found to be considerably smaller than 1 (Rose et
1038 al., 2010; Gunthe et al., 2011; Che et al., 2017; Zhang et al., 2017), especially at low
1039 supersaturation, and CCN-inactive particles were usually attributed to low hygroscopic primary
1040 particles (e.g., soot) from local sources. The average κ , reported by previous studies, were
1041 generally found to be in the range of 0.30-0.35; however, CCN activities could be significantly
1042 reduced if measurement sites were affected by fresh urban pollution or biomass burning (Rose et
1043 al., 2010; Gunthe et al., 2011; Zhang et al., 2014; Wu et al., 2017), due to enhanced contribution
1044 of soot and organics. **We note that a few recent studies (Atwood et al., 2017; Zhang et al., 2017;**
1045 **Cai et al., 2020) also reported higher aerosol hygroscopicity. For example,** the average κ observed
1046 at the Xinzhou site appeared to be larger than those reported at other continental site (Zhang et al.,
1047 2017), probably because aerosols arriving at this site were heavily aged; in addition, two studies
1048 which investigated aerosol CCN activities in the marine boundary layer reported larger κ values
1049 (Atwood et al., 2017; Cai et al., 2020), compared to those at continental sites.



1050

1051 **Figure 7.** Measured κ_a as a function of particle diameter reported by previous studies (Rose et al.,
1052 2010; Deng et al., 2011; Gunthe et al., 2011; Deng et al., 2013; Meng et al., 2014; Zhang et al.,
1053 2014; Che et al., 2016; Ma et al., 2016; Che et al., 2017; Ma et al., 2017; Zhang et al., 2017; Cai
1054 et al., 2018; Tao et al., 2020) in the NCP (a) and other regions in China (b). Solid symbols represent
1055 urban/suburban sites, and open symbols represent rural sites.

1056

1057 Figure 7 summarizes size dependence of κ_a reported by CCN measurements at continental sites
1058 in China, and measurement data related to specific cases (e.g., biomass burning events) are not
1059 included (Rose et al., 2010; Wu et al., 2017). As shown in Figure 7, in general κ_a increased with
1060 particle size, as mass fractions increased with particle size for soluble inorganics and decreased for
1061 organics. Nevertheless, no obvious dependence of κ_a on particle size was also observed in Xinzhou

1062 (Zhang et al., 2017) and Nanjing (Ma et al., 2017), probably because aerosol particles at these two
1063 sites were substantially aged and thus very well internally mixed.

1064 Several studies carried out CCN activity closure analysis. Some studies suggested that the
1065 measured κ could be well quantitatively explained by aerosol composition (Rose et al., 2010;
1066 Gunthe et al., 2011; Wu et al., 2017), while other studies showed that κ estimated using aerosol
1067 composition were either larger (Zhang et al., 2017) or smaller than measured values (Zhang et al.,
1068 2017; Cai et al., 2018). In addition, a few studies investigated aerosol hygroscopic growth and
1069 CCN activities concurrently, and both **consistencies** (Wu et al., 2017; Zhang et al., 2017; Cai et al.,
1070 2018) and discrepancies (Ma et al., 2016; Zhang et al., 2016b) were reported. **The discrepancies**
1071 **could be caused by several factors (Petters and Kreidenweis, 2008; Wex et al., 2009; Petters and**
1072 **Kreidenweis, 2013; Liu et al., 2018b)**, such as solution non-ideality of aerosol droplets, limited
1073 **solubility of some components contained by aerosol particles, surface tension effects, and etc.**

1074 **5 Perspectives**

1075 In the last 10-20 years a number of field measurements of hygroscopic properties and CCN
1076 activities of tropospheric aerosols have been carried out in China, and summaries of measured
1077 hygroscopic properties and CCN activities are provided in Sections 3.5 and 4.5. As shown in
1078 Sections 3 and 4, these studies have significantly improved our knowledge of tropospheric aerosol
1079 hygroscopicity in China and provided valuable data to better understand the roles aerosols play in
1080 heterogeneous and multiphase chemistry, as well as direct and indirect radiative forcing. However,
1081 large knowledge gaps still exist for aerosol hygroscopicity in China, as described below, and future
1082 research directions are also **proposed**.

1083 **Data availability:** In Tables S1-S5 we attempt to compile measurement data reported by
1084 previous studies under a consistent framework in order to enhance their accessibility and usability.

1085 However, important data are not always available from every study published; for example, several
1086 studies presented their main results graphically. It is recommended that in future data in the
1087 numerical form (H-TDMA measurements: including but not limited to diameter, RH, and GF
1088 and/or κ ; CCN activity measurements: including but not limited to supersaturation, activation
1089 diameter and κ) should be provided.

1090 **Geographical coverages:** As shown in Sections 3-4, almost all the measurements of
1091 hygroscopic properties and CCN activities in China were carried out in **eastern** regions (e.g., NCP,
1092 YRD and PRD) heavily affected by anthropogenic emissions. Therefore, it will be very desirable
1093 in future to carry out these measurements in other regions; measurements in areas far from by
1094 human activities will be especially important, as they will provide information on aerosol
1095 hygroscopicity in the **cleaner** troposphere.

1096 **Vertical distribution:** Most of previous aerosol hygroscopicity measurements in China were
1097 only carried out at or close to the ground level. However, both aerosol composition and RH, and
1098 as a result aerosol hygroscopic growth and CCN activation, will vary with altitude. For example,
1099 aircraft-based measurements of aerosol size distribution and composition indicated that single
1100 hygroscopicity parameters would increase significantly with altitude (Liu et al., 2020), and it was
1101 revealed from remote sensing that aerosol hygroscopicity at the upper boundary level was different
1102 from that at the ground level (Tan et al., 2020). Therefore, in-situ measurements of vertical profiles
1103 of aerosol composition and hygroscopicity on different platforms (e.g., towers, airships, aircrafts,
1104 and etc.) will be very valuable; in addition, remote sensing may be very useful for retrieving
1105 vertical profiles of aerosol hygroscopicity, as demonstrated by a very recent study (Tan et al., 2020).

1106 **Long-term measurements:** Both aerosol concentration and composition have undergone (and
1107 very likely will undergo) significant changes in China; however, most aerosol hygroscopicity

1108 measurements were carried out for 1-2 months during specific field campaigns. Long-term
1109 measurements of aerosol hygroscopicity will be very important to understand seasonal and annual
1110 variations of aerosol hygroscopicity and the implications for visibility, atmospheric chemistry and
1111 climate change.

1112 **Hygroscopicity of large particles:** Tables S1-S4 reveal that the maximum aerosol diameter
1113 examined in hygroscopic growth studies was 350 nm, which is the upper limit of dry aerosol size
1114 for most of H-TDMA instruments (Tang et al., 2019). As particles larger than 350 nm can
1115 contribute substantially to aerosol surface area and volume (or mass) concentrations,
1116 hygroscopicity of these particles will be very important and should be measured in future, and this
1117 requires technical improvements of H-TDMA. On the other hand, hygroscopicity of >350 nm
1118 particles may not be very important for CCN activation, as these particles can be easily activated
1119 **at low supersaturation** due to their **size**.

1120 **RH dependence:** Most H-TDMA measurements were carried out at a single RH (usually
1121 ~90%), and a few studies which measured GF as a function of RH suggested that a constant κ
1122 failed to describe hygroscopic growth at different RH. In addition, due to lack of measurement
1123 data at different RH, it is not clear how well widely-used aerosol thermodynamic models can
1124 simulate ALWC at ambient RH. Therefore, measurements of aerosol hygroscopicity at different
1125 RH are certainly warranted, **and hygroscopic growth factors measured at high RH (at 90% RH or**
1126 **above) are preferably used to calculate κ values.**

1127 **The effect of aerosol organics:** As discussed in Section 3, several studies (Liu et al., 2014;
1128 Wu et al., 2016; Cai et al., 2018; Hong et al., 2018; Li et al., 2019b; Jin et al., 2020) suggested that
1129 organics contributed substantially to aerosol water uptake, while some studies also indicated that
1130 the contribution of aerosol organics to ALWC was rather minor. Therefore, aerosol hygroscopicity

1131 closure analysis, with concurrent measurements of aerosol composition and hygroscopicity, is
1132 recommended for future, in order to further understand the effects of aerosol organics on ALWC
1133 and CCN activation; in addition, relevant factors which need consideration include the dependence
1134 of hygroscopicity on composition of aerosol organics (e.g., O/C ratios) and the effects of aerosol
1135 organics on surface tension, phase separation effects, and etc.

1136

1137 **Data Availability.** This is a review paper, and all the data used come from cited literature. In
1138 addition, the data we have compiled can be found in the supplement.

1139 **Author contribution.** Mingjin Tang conceived this work; Chao Peng and Mingjin Tang wrote the
1140 manuscript with substantial input from Yu Wang, Zhijun Wu and Lanxiadi Chen; all the authors
1141 revised the manuscript and approved its submission.

1142 **Conflict of Interest.** The authors declare no conflict of interest.

1143 **Acknowledgment.** We would like to thank participants in the fifth International Workshop on
1144 Heterogeneous Kinetics Related to Atmospheric Aerosols for discussion.

1145 **Financial support.** This work was funded by National Natural Science Foundation of China
1146 (91744204 and 91844301), State Key Laboratory of Loess and Quaternary Geology
1147 (SKLLQG1921), Department of Science and Technology of Guangdong Province
1148 (2017GC010501), and Guangdong Foundation for Program of Science and Technology Research
1149 (2017B030314057 and 2019B121205006). Mingjin Tang would like to thank the CAS Pioneer
1150 Hundred Talents program for providing a starting grant.

1151

1152 **Reference**

1153 Achtert, P., Birmili, W., Nowak, A., Wehner, B., Wiedensohler, A., Takegawa, N., Kondo, Y., Miyazaki, Y., Hu, M.,
1154 and Zhu, T.: Hygroscopic growth of tropospheric particle number size distributions over the North China Plain,
1155 Journal of Geophysical Research-Atmospheres, 114, D00G07, 10.1029/2008JD010921, 2009.

1156 An, Z., Huang, R.-J., Zhang, R., Tie, X., Li, G., Cao, J., Zhou, W., Shi, Z., Han, Y., Gu, Z., and Ji, Y.: Severe haze in
1157 northern China: A synergy of anthropogenic emissions and atmospheric processes, *Proceedings of the National*
1158 *Academy of Sciences of the United States of America*, 116, 8657-8666, 2019.

1159 Asmi, E., Frey, A., Virkkula, A., Ehn, M., Manninen, H. E., Timonen, H., Tolonen-Kivimaki, O., Aurela, M., Hillamo,
1160 R., and Kulmala, M.: Hygroscopicity and chemical composition of Antarctic sub-micrometre aerosol particles
1161 and observations of new particle formation, *Atmospheric Chemistry and Physics*, 10, 4253-4271, 2010.

1162 Atwood, S. A., Reid, J. S., Kreidenweis, S. M., Blake, D. R., Jonsson, H. H., Lagrosas, N. D., Xian, P., Reid, E. A.,
1163 Sessions, W. R., and Simpas, J. B.: Size-resolved aerosol and cloud condensation nuclei (CCN) properties in the
1164 remote marine South China Sea - Part 1: Observations and source classification, *Atmospheric Chemistry and*
1165 *Physics*, 17, 1105-1123, 2017.

1166 Bedoya-Velásquez, A. E., Navas-Guzmán, F., Jose Granados-Muñoz, M., Titos, G., Román, R., Andres Casquero-Vera,
1167 J., Ortiz-Amezcu, P., Antonio Benavent-Oltra, J., de Arruda Moreira, G., Montilla-Rosero, E., David Hoyos, C.,
1168 Artiñano, B., Coz, E., Jose Olmo-Reyes, F., Alados-Arboledas, L., and Luis Guerrero-Rascado, J.: Hygroscopic
1169 growth study in the framework of EARLINET during the SLOPE I campaign: synergy of remote sensing and in
1170 situ instrumentation, *Atmospheric Chemistry and Physics*, 18, 7001-7017, 2018.

1171 Bertram, T. H., and Thornton, J. A.: Toward a general parameterization of N_2O_5 reactivity on aqueous particles: the
1172 competing effects of particle liquid water, nitrate and chloride, *Atmospheric Chemistry And Physics*, 9, 8351-
1173 8363, 2009.

1174 Bian, Y. X., Zhao, C. S., Ma, N., Chen, J., and Xu, W. Y.: A study of aerosol liquid water content based on
1175 hygroscopicity measurements at high relative humidity in the North China Plain, *Atmospheric Chemistry and*
1176 *Physics*, 14, 6417-6426, 2014.

1177 Bougiatioti, A., Nenes, A., Fountoukis, C., Kalivitis, N., Pandis, S. N., and Mihalopoulos, N.: Size-resolved CCN
1178 distributions and activation kinetics of aged continental and marine aerosol, *Atmospheric Chemistry and Physics*,
1179 11, 8791-8808, 2011.

1180 Burgos, M. A., Andrews, E., Titos, G., Alados-Arboledas, L., Baltensperger, U., Day, D., Jefferson, A., Kalivitis, N.,
1181 Mihalopoulos, N., Sherman, J., Sun, J., Weingartner, E., and Zieger, P.: A global view on the effect of water
1182 uptake on aerosol particle light scattering, *Scientific Data*, 6, 157, 2019.

1183 Burkart, J., Steiner, G., Reischl, G., and Hitzenberger, R.: Long-term study of cloud condensation nuclei (CCN)
1184 activation of the atmospheric aerosol in Vienna, *Atmospheric Environment*, 45, 5751-5759, 2011.

1185 Cai, M., Tan, H., Chan, C. K., Mochida, M., Hatakeyama, S., Kondo, Y., Schurman, M. I., Xu, H., Li, F., Shimada, K.,
1186 Li, L., Deng, Y., Yai, H., Matsuki, A., Qin, Y., and Zhao, J.: Comparison of Aerosol Hygroscopicity, Volatility, and
1187 Chemical Composition between a Suburban Site in the Pearl River Delta Region and a Marine Site in Okinawa,
1188 *Aerosol and Air Quality Research*, 17, 3194-3208, 2017.

1189 Cai, M., Tan, H., Chan, C. K., Qin, Y., Xu, H., Li, F., Schurman, M. I., Liu, L., and Zhao, J.: The size-resolved cloud
1190 condensation nuclei (CCN) activity and its prediction based on aerosol hygroscopicity and composition in the
1191 Pearl Delta River (PRD) region during wintertime 2014, *Atmospheric Chemistry and Physics*, 18, 16419-16437,
1192 2018.

1193 Cai, M., Liang, B., Sun, Q., Zhou, S., Yuan, B., Shao, M., Tan, H., and Zhao, J.: Effects of continental emissions on
1194 Cloud Condensation Nuclei (CCN) activity in northern South China Sea during summertime 2018, *Atmospheric*
1195 *Chemistry and Physics Discussions*, 2020, 1-43, 2020.

1196 Cerully, K. M., Raatikainen, T., Lance, S., Tkacik, D., Tiipta, P., Petäjä, T., Ehn, M., Kulmala, M., Worsnop, D. R.,
1197 Laaksonen, A., Smith, J. N., and Nenes, A.: Aerosol hygroscopicity and CCN activation kinetics in a boreal forest
1198 environment during the 2007 EUCAARI campaign, *Atmos. Chem. Phys.*, 11, 12369-12386, 2011.

1199 Che, H. C., Zhang, X. Y., Wang, Y. Q., Zhang, L., Shen, X. J., Zhang, Y. M., Ma, Q. L., Sun, J. Y., Zhang, Y. W., and
1200 Wang, T. T.: Characterization and parameterization of aerosol cloud condensation nuclei activation under
1201 different pollution conditions, *Scientific reports*, 6, 24497, 24410.21038/srep24497, 2016.

1202 Che, H. C., Zhang, X. Y., Zhang, L., Wang, Y. Q., Zhang, Y. M., Shen, X. J., Ma, Q. L., Sun, J. Y., and Zhong, J. T.:
1203 Prediction of size-resolved number concentration of cloud condensation nuclei and long-term measurements of
1204 their activation characteristics, *Scientific reports*, 7, 5819, 5810.1038/s41598-41017-05998-41593, 2017.

1205 Chen, H., Yang, S., Li, Y., Yin, Y., Zhang, Z., Yu, X., Kang, N., Yan, S., and Xia, H.: Hygroscopic Properties and
1206 Closure of Aerosol Chemical Composition in Mt. Huang in Summer (in Chinese), *Environmental Science*, 37,
1207 2008-2016, 2016.

1208 Chen, J., Li, Z., Lv, M., Wang, Y., Wang, W., Zhang, Y., Wang, H., Yan, X., Sun, Y., and Cribb, M.: Aerosol hygroscopic
1209 growth, contributing factors, and impact on haze events in a severely polluted region in northern China,
1210 *Atmospheric Chemistry and Physics*, 19, 1327-1342, 2019.

1211 Chen, L. Y., Jeng, F. T., Chen, C. C., and Hsiao, T. C.: Hygroscopic behavior of atmospheric aerosol in Taipei,
1212 Atmospheric Environment, 37, 2069-2075, 2003.

1213 Cheng, Y. F., Eichler, H., Wiedensohler, A., Heintzenberg, J., Zhang, Y. H., Hu, M., Herrmann, H., Zeng, L. M., Liu,
1214 S., Gnauk, T., Brueggemann, E., and He, L. Y.: Mixing state of elemental carbon and non-light-absorbing aerosol
1215 components derived from in situ particle optical properties at Xinken in Pearl River Delta of China, Journal of
1216 Geophysical Research-Atmospheres, 111, D20204, 20210.21029/22005JD006929, 2006.

1217 Cheung, H. H. Y., Yeung, M. C., Li, Y. J., Lee, B. P., and Chan, C. K.: Relative Humidity- Dependent HTDMA
1218 Measurements of Ambient Aerosols at the HKUST Supersite in Hong Kong, China, Aerosol Science and
1219 Technology, 49, 643-654, 2015.

1220 Chu, B. W., Ma, Q. X., Duan, F. K., Ma, J. Z., Jiang, J. K., He, K. B., and He, H.: Atmospheric "Haze Chemistry":
1221 Concept and Research Prospects, Progress in Chemistry, 32, 1-4, 2020.

1222 Chuang, P. Y., Nenes, A., Smith, J. N., Flagan, R. C., and Seinfeld, J. H.: Design of a CCN instrument for airborne
1223 measurement, Journal of Atmospheric and Oceanic Technology, 17, 1005-1019, 2000.

1224 Cocker, D. R., Whitlock, N. E., Flagan, R. C., and Seinfeld, J. H.: Hygroscopic properties of Pasadena, California
1225 aerosol, Aerosol Science and Technology, 35, 637-647, 2001.

1226 Cubison, M. J., Coe, H., and Gysel, M.: A modified hygroscopic tandem DMA and a data retrieval method based on
1227 optimal estimation, Journal of Aerosol Science, 36, 846-865, 2005.

1228 Dawson, K. W., Ferrare, R. A., Moore, R. H., Clayton, M. B., Thorsen, T. J., and Eloranta, E. W.: Ambient Aerosol
1229 Hygroscopic Growth From Combined Raman Lidar and HSRL, Journal of Geophysical Research-Atmospheres,
1230 125, 031708, 031710.031029/032019JD031708, 2020.

1231 Deng, Z. Z., Zhao, C. S., Ma, N., Liu, P. F., Ran, L., Xu, W. Y., Chen, J., Liang, Z., Liang, S., Huang, M. Y., Ma, X.
1232 C., Zhang, Q., Quan, J. N., Yan, P., Henning, S., Mildenberger, K., Sommerhage, E., Schaefer, M., Stratmann, F.,
1233 and Wiedensohler, A.: Size-resolved and bulk activation properties of aerosols in the North China Plain,
1234 Atmospheric Chemistry and Physics, 11, 3835-3846, 2011.

1235 Deng, Z. Z., Zhao, C. S., Ma, N., Ran, L., Zhou, G. Q., Lu, D. R., and Zhou, X. J.: An examination of parameterizations
1236 for the CCN number concentration based on in situ measurements of aerosol activation properties in the North
1237 China Plain, Atmospheric Chemistry and Physics, 13, 6227-6237, 2013.

1238 Ding, J., Zhang, Y. F., Zhao, P. S., Tang, M., Xiao, Z. M., Zhang, W. H., Zhang, H. T., Yu, Z. J., Du, X., Li, L. W.,
1239 Yuan, J., and Feng, Y. C.: Comparison of size-resolved hygroscopic growth factors of urban aerosol by different
1240 methods in Tianjin during a haze episode, Science of the Total Environment, 678, 618-626, 2019.

1241 Duan, J., Tao, J., Wu, Y., Cheng, T., Zhang, R., Wang, Y., Zhu, H., Xie, X., Liu, Y., Li, X., Kong, L., Li, M., and He,
1242 Q.: Comparison of aerosol and cloud condensation nuclei between wet and dry seasons in Guangzhou, southern
1243 China, Science of the Total Environment, 607, 11-22, 2017.

1244 Duan, J., Wang, Y., Xie, X., Li, M., Tao, J., Wu, Y., Cheng, T., Zhang, R., Liu, Y., Li, X., He, Q., Gao, W., and Wang,
1245 J.: Influence of pollutants on activity of aerosol cloud condensation nuclei (CCN) during pollution and post-rain
1246 periods in Guangzhou, southern China, Science of the Total Environment, 642, 1008-1019, 2018.

1247 Duplissy, J., Gysel, M., Sjogren, S., Meyer, N., Good, N., Kammermann, L., Michaud, V., Weigel, R., dos Santos, S.
1248 M., Gruening, C., Villani, P., Laj, P., Sellegrí, K., Metzger, A., McFiggans, G. B., Wehrle, G., Richter, R.,
1249 Dommen, J., Ristovski, Z., Baltensperger, U., and Weingartner, E.: Intercomparison study of six HTDMAs:
1250 results and recommendations, Atmospheric Measurement Techniques, 2, 363-378, 2009.

1251 Dusek, U., Frank, G. P., Hildebrandt, L., Curtius, J., Schneider, J., Walter, S., Chand, D., Drewnick, F., Hings, S., Jung,
1252 D., Borrmann, S., and Andreae, M. O.: Size matters more than chemistry for cloud-nucleating ability of aerosol
1253 particles, Science, 312, 1375-1378, 2006.

1254 Eichler, H., Cheng, Y. F., Birmili, W., Nowak, A., Wiedensohler, A., Brueggemann, E., Gnauk, T., Herrmann, H.,
1255 Althausen, D., Ansmann, A., Engelmann, R., Tesche, M., Wendisch, M., Zhang, Y. H., Hu, M., Liu, S., and Zeng,
1256 L. M.: Hygroscopic properties and extinction of aerosol particles at ambient relative humidity in South-Eastern
1257 China, Atmospheric Environment, 42, 6321-6334, 2008.

1258 Fajardo, O. A., Jiang, J., and Hao, J.: Continuous Measurement of Ambient Aerosol Liquid Water Content in Beijing,
1259 Aerosol and Air Quality Research, 16, 1152-1164, 2016.

1260 Fan, X., Liu, J., Zhang, F., Chen, L., Collins, D., Xu, W., Jin, X., Ren, J., Wang, Y., Wu, H., Li, S., Sun, Y., and Li, Z.:
1261 Contrasting size-resolved hygroscopicity of fine particles derived by HTDMA and HR-ToF-AMS measurements
1262 between summer and winter in Beijing: the impacts of aerosol aging and local emissions, Atmospheric Chemistry
1263 and Physics, 20, 915-929, 2020.

1264 Fang, S., Han, Y., Chen, K., Lu, C., Yin, Y., Tan, H., and Wang, J.: Parameterization and comparative evaluation of
1265 the CCN number concentration on Mt. Huang, China, Atmospheric Research, 181, 300-311, 2016.

1266 Farmer, D. K., Cappa, C. D., and Kreidenweis, S. M.: Atmospheric processes and their controlling influence on cloud
1267 condensation nuclei activity, *Chem Rev*, 115, 4199-4217, 2015.

1268 Frank, G. P., Dusek, U., and Andreae, M. O.: Technical note: Characterization of a static thermal-gradient CCN counter,
1269 *Atmospheric Chemistry and Physics*, 7, 3071-3080, 2007.

1270 Fukuta, N., and Saxena, V. K.: HORIZONTAL THERMAL-GRADIENT CLOUD CONDENSATION NUCLEUS
1271 SPECTROMETER, *Journal of Applied Meteorology*, 18, 1352-1362, 1979.

1272 Gao, Y., Zhang, D., Wang, J., Gao, H., and Yao, X.: Variations in Ncn and Ncen over China marginal seas related to
1273 marine traffic emissions, new particle formation and aerosol aging, *Atmospheric Chemistry and Physics*
1274 Discussions, 2020, 1-37, 2020.

1275 Good, N., Coe, H., and McFiggans, G.: Instrumentational operation and analytical methodology for the reconciliation
1276 of aerosol water uptake under sub- and supersaturated conditions, *Atmospheric Measurement Techniques*, 3,
1277 1241-1254, 2010.

1278 Gunthe, S. S., Rose, D., Su, H., Garland, R. M., Achtert, P., Nowak, A., Wiedensohler, A., Kuwata, M., Takegawa, N.,
1279 Kondo, Y., Hu, M., Shao, M., Zhu, T., Andreae, M. O., and Poeschl, U.: Cloud condensation nuclei (CCN) from
1280 fresh and aged air pollution in the megacity region of Beijing, *Atmospheric Chemistry and Physics*, 11, 11023-
1281 11039, 2011.

1282 Guo, S., Hu, M., Zamora, M. L., Peng, J., Shang, D., Zheng, J., Du, Z., Wu, Z., Shao, M., and Zeng, L.: Elucidating
1283 severe urban haze formation in China, *Proceedings of the National Academy of Sciences*, 111, 17373-17378,
1284 2014.

1285 Gysel, M., Crosier, J., Topping, D. O., Whitehead, J. D., Bower, K. N., Cubison, M. J., Williams, P. I., Flynn, M. J.,
1286 McFiggans, G. B., and Coe, H.: Closure study between chemical composition and hygroscopic growth of aerosol
1287 particles during TORCH2, *Atmospheric Chemistry and Physics*, 7, 6131-6144, 2007.

1288 Gysel, M., McFiggans, G. B., and Coe, H.: Inversion of tandem differential mobility analyser (TDMA) measurements,
1289 *Journal of Aerosol Science*, 40, 134-151, 2009.

1290 He, H., Wang, Y., Ma, Q., Ma, J., Chu, B., Ji, D., Tang, G., Liu, C., Zhang, H., and Hao, J.: Mineral dust and NOx
1291 promote the conversion of SO2 to sulfate in heavy pollution days, *Scientific reports*, 4, 4172, 2014.

1292 Hong, J., Xu, H., Tan, H., Yin, C., Hao, L., Li, F., Cai, M., Deng, X., Wang, N., Su, H., Cheng, Y., Wang, L., Petaja,
1293 T., and Kerminen, V.-M.: Mixing state and particle hygroscopicity of organic-dominated aerosols over the Pearl
1294 River Delta region in China, *Atmospheric Chemistry and Physics*, 18, 14079-14094, 2018.

1295 Huang, R.-J., Zhang, Y., Bozzetti, C., Ho, K.-F., Cao, J.-J., Han, Y., Daellenbach, K. R., Slowik, J. G., Platt, S. M.,
1296 and Canonaco, F.: High secondary aerosol contribution to particulate pollution during haze events in China,
1297 *Nature*, 514, 218, 2014.

1298 Hudson, J. G.: AN INSTANTANEOUS CCN SPECTROMETER, *Journal of Atmospheric and Oceanic Technology*,
1299 6, 1055-1065, 1989.

1300 Hung, H.-M., Lu, W.-J., Chen, W.-N., Chang, C.-C., Chou, C. C. K., and Lin, P.-H.: Enhancement of the hygroscopicity
1301 parameter kappa of rural aerosols in northern Taiwan by anthropogenic emissions, *Atmospheric Environment*,
1302 84, 78-87, 2014.

1303 Hung, H.-M., Hsu, C.-H., Lin, W.-T., and Chen, Y.-Q.: A case study of single hygroscopicity parameter and its link to
1304 the functional groups and phase transition for urban aerosols in Taipei City, *Atmospheric Environment*, 132, 240-
1305 248, 2016.

1306 Ji, Q., Shaw, G. E., and Cantrell, W.: A new instrument for measuring cloud condensation nuclei: Cloud condensation
1307 nucleus "remover", *Journal of Geophysical Research-Atmospheres*, 103, 28013-28019, 1998.

1308 Jiang, R., Tan, H., Tang, L., Cai, M., Yin, Y., Li, F., Liu, L., Xu, H., Chan, P. W., Deng, X., and Wu, D.: Comparison
1309 of aerosol hygroscopicity and mixing state between winter and summer seasons in Pearl River Delta region,
1310 China, *Atmospheric Research*, 169, 160-170, 2016.

1311 Jin, X., Wang, Y., Li, Z., Zhang, F., Xu, W., Sun, Y., Fan, X., Chen, G., Wu, H., Ren, J., Wang, Q., and Cribb, M.:
1312 Significant contribution of organics to aerosol liquid water content in winter in Beijing, China, *Atmospheric
1313 Chemistry and Physics*, 20, 901-914, 2020.

1314 Kim, J.-S., Kim, Y. J., and Park, K.: Measurements of hygroscopicity and volatility of atmospheric ultrafine particles
1315 in the rural Pearl River Delta area of China, *Atmospheric Environment*, 45, 4661-4670, 2011.

1316 King, S. M., Rosenoern, T., Shilling, J. E., Chen, Q., and Martin, S. T.: Increased cloud activation potential of
1317 secondary organic aerosol for atmospheric mass loadings, *Atmospheric Chemistry and Physics*, 9, 2959-2971,
1318 2009.

1319 Kreidenweis, S. M., Koehler, K., DeMott, P. J., Prenni, A. J., Carrico, C., and Ervens, B.: Water activity and activation
1320 diameters from hygroscopicity data - Part I: Theory and application to inorganic salts, *Atmospheric Chemistry
1321 and Physics*, 5, 1357-1370, 2005.

1322 Kreidenweis, S. M., and Asa-Awuku, A.: 5.13 - Aerosol Hygroscopicity: Particle Water Content and Its Role in
1323 Atmospheric Processes, in: Treatise on Geochemistry (Second Edition), edited by: Turekian, K. K., Elsevier,
1324 Oxford, 331-361, 2014.

1325 Krieger, U. K., Marcolli, C., and Reid, J. P.: Exploring the complexity of aerosol particle properties and processes
1326 using single particle techniques, *Chemical Society Reviews*, 41, 6631-6662, 2012.

1327 Kuang, Y., Zhao, C., Tao, J., Bian, Y., Ma, N., and Zhao, G.: A novel method for deriving the aerosol hygroscopicity
1328 parameter based only on measurements from a humidified nephelometer system, *Atmospheric Chemistry and*
1329 *Physics*, 17, 6651-6662, 2017.

1330 Kuang, Y., Zhao, C. S., Zhao, G., Tao, J. C., Xu, W., Ma, N., and Bian, Y. X.: A novel method for calculating ambient
1331 aerosol liquid water content based on measurements of a humidified nephelometer system, *Atmospheric*
1332 *Measurement Techniques*, 11, 2967-2982, 2018.

1333 Lance, S., Medina, J., Smith, J. N., and Nenes, A.: Mapping the operation of the DMT Continuous Flow CCN counter,
1334 *Aerosol Science and Technology*, 40, 242-254, 2006.

1335 Leng, C., Cheng, T., Chen, J., Zhang, R., Tao, J., Huang, G., Zha, S., Zhang, M., Fang, W., Li, X., and Li, L.:
1336 Measurements of surface cloud condensation nuclei and aerosol activity in downtown Shanghai, *Atmospheric*
1337 *Environment*, 69, 354-361, 2013.

1338 Leng, C., Zhang, Q., Zhang, D., Xu, C., Cheng, T., Zhang, R., Tao, J., Chen, J., Zha, S., Zhang, Y., Li, X., Kong, L.,
1339 and Gao, W.: Variations of cloud condensation nuclei (CCN) and aerosol activity during fog-haze episode: a case
1340 study from Shanghai, *Atmospheric Chemistry and Physics*, 14, 12499-12512, 2014.

1341 Li, K., Zhu, Y., Gao, H., and Yao, X.: A comparative study of cloud condensation nuclei measured between non-
1342 heating and heating periods at a suburb site of Qingdao in the North China, *Atmospheric Environment*, 112, 40-
1343 53, 2015a.

1344 Li, K., Ye, X., Pang, H., Lu, X., Chen, H., Wang, X., Yang, X., Chen, J., and Chen, Y.: Temporal variations in the
1345 hygroscopicity and mixing state of black carbon aerosols in a polluted megacity area, *Atmospheric Chemistry*
1346 and Physics, 18, 15201-15218, 2018.

1347 Li, K., Jacob, D. J., Liao, H., Shen, L., Zhang, Q., and Bates, K. H.: Anthropogenic drivers of 2013-2017 trends in
1348 summer surface ozone in China, *Proceedings of the National Academy of Sciences of the United States of*
1349 *America*, 116, 422-427, 2019a.

1350 Li, M., Liu, H., Geng, G., Hong, C., Liu, F., Song, Y., Tong, D., Zheng, B., Cui, H., Man, H., Zhang, Q., and He, K.:
1351 Anthropogenic emission inventories in China: a review, *National Science Review*, 4, 834-866, 2017a.

1352 Li, Q., Yin, Y., Gu, X., Yuan, L., Kong, S., Jiang, Q., Chen, K., and Li, L.: An observational study of aerosol
1353 hygroscopic growth factor and cloud condensation nuclei in Nanjing in summer (in Chinese), *China*
1354 *Environmental Science*, 35, 337-346, 2015b.

1355 Li, W., Shao, L., Zhang, D., Ro, C.-U., Hu, M., Bi, X., Geng, H., Matsuki, A., Niu, H., and Chen, J.: A review of single
1356 aerosol particle studies in the atmosphere of East Asia: morphology, mixing state, source, and heterogeneous
1357 reactions, *Journal of Cleaner Production*, 112, 1330-1349, 2016.

1358 Li, X., Song, S., Zhou, W., Hao, J., Worsnop, D. R., and Jiang, J.: Interactions between aerosol organic components
1359 and liquid water content during haze episodes in Beijing, *Atmospheric Chemistry and Physics*, 19, 12163-12174,
1360 2019b.

1361 Li, Y., Zhang, F., Li, Z., Sun, L., Wang, Z., Li, P., Sun, Y., Ren, J., Wang, Y., Cribb, M., and Yuan, C.: Influences of
1362 aerosol physiochemical properties and new particle formation on CCN activity from observation at a suburban
1363 site of China, *Atmospheric Research*, 188, 80-89, 2017b.

1364 Liu, B. Y. H., Pui, D. Y. H., Whitby, K. T., Kittelson, D. B., Kousaka, Y., and McKenzie, R. L.: AEROSOL MOBILITY
1365 CHROMATOGRAPH - NEW DETECTOR FOR SULFURIC-ACID AEROSOLS, *Atmospheric Environment*,
1366 12, 99-104, 1978.

1367 Liu, H. J., Zhao, C. S., Nekat, B., Ma, N., Wiedensohler, A., van Pinxteren, D., Spindler, G., Mueller, K., and Herrmann,
1368 H.: Aerosol hygroscopicity derived from size-segregated chemical composition and its parameterization in the
1369 North China Plain, *Atmospheric Chemistry and Physics*, 14, 2525-2539, 2014.

1370 Liu, L., Tan, H., Fan, S., Cai, M., Xu, H., Li, F., and Chan, P.: Influence of aerosol hygroscopicity and mixing state on
1371 aerosol optical properties in the Pearl River Delta region, China, *Science of the Total Environment*, 627, 1560-
1372 1571, 2018a.

1373 Liu, P., Song, M., Zhao, T., Gunthe, S. S., Ham, S., He, Y., Qin, Y. M., Gong, Z., Amorim, J. C., Bertram, A. K., and
1374 Martin, S. T.: Resolving the mechanisms of hygroscopic growth and cloud condensation nuclei activity for
1375 organic particulate matter, *Nature Communications*, 9, 2018b.

1376 Liu, P. F., Zhao, C. S., Goebel, T., Hallbauer, E., Nowak, A., Ran, L., Xu, W. Y., Deng, Z. Z., Ma, N., Mildenberger,
1377 K., Henning, S., Stratmann, F., and Wiedensohler, A.: Hygroscopic properties of aerosol particles at high relative

1378 humidity and their diurnal variations in the North China Plain, *Atmospheric Chemistry and Physics*, 11, 3479-
 1379 3494, 2011.

1380 Liu, Q., Liu, D., Gao, Q., Tian, P., Wang, F., Zhao, D., Bi, K., Wu, Y., Ding, S., Hu, K., Zhang, J., Ding, D., and Zhao,
 1381 C.: Vertical characteristics of aerosol hygroscopicity and impacts on optical properties over the North China Plain
 1382 during winter, *Atmospheric Chemistry and Physics*, 20, 3931-3944, 2020.

1383 Liu, Y., Wu, Z., Wang, Y., Xiao, Y., Gu, F., Zheng, J., Tan, T., Shang, D., Wu, Y., Zeng, L., Hu, M., Bateman, A. P.,
 1384 and Martin, S. T.: Submicrometer Particles Are in the Liquid State during Heavy Haze Episodes in the Urban
 1385 Atmosphere of Beijing, China, *Environmental Science & Technology Letters*, 4, 427-432, 2017.

1386 Lopez-Yglesias, X. F., Yeung, M. C., Dey, S. E., Brechtel, F. J., and Chan, C. K.: Performance Evaluation of the
 1387 Brechtel Mfg. Humidified Tandem Differential Mobility Analyzer (BMI HTDMA) for Studying Hygroscopic
 1388 Properties of Aerosol Particles, *Aerosol Science and Technology*, 48, 969-980, 2014.

1389 Lu, G., and Guo, X.: Distribution and origin of aerosol and its transform relationship with CCN derived from the
 1390 spring multi-aircraft measurements of Beijing Cloud Experiment (BCE), *Chinese Science Bulletin*, 57, 2460-
 1391 2469, 2012.

1392 Lu, K., Guo, S., Tan, Z., Wang, H., Shang, D., Liu, Y., Li, X., Wu, Z., Hu, M., and Zhang, Y.: Exploring atmospheric
 1393 free-radical chemistry in China: the self-cleansing capacity and the formation of secondary air pollution, *National
 1394 Science Review*, 6, 579-594, 2019.

1395 Lu, X., Zhang, L., Wang, X., Gao, M., Li, K., Zhang, Y., Yue, X., and Zhang, Y.: Rapid Increases in Warm-Season
 1396 Surface Ozone and Resulting Health Impact in China Since 2013, *Environmental Science & Technology Letters*,
 1397 7, 240-247, 2020.

1398 Lv, M., Liu, D., Li, Z., Mao, J., Sun, Y., Wang, Z., Wang, Y., and Xie, C.: Hygroscopic growth of atmospheric aerosol
 1399 particles based on lidar, radiosonde, and in situ measurements: Case studies from the Xinzhou field campaign,
 1400 *Journal of Quantitative Spectroscopy & Radiative Transfer*, 188, 60-70, 2017.

1401 Ma, N., Zhao, C., Tao, J., Wu, Z., Kecorius, S., Wang, Z., Groess, J., Liu, H., Bian, Y., Kuang, Y., Teich, M., Spindler,
 1402 G., Mueller, K., van Pinxteren, D., Herrmann, H., Hu, M., and Wiedensohler, A.: Variation of CCN activity during
 1403 new particle formation events in the North China Plain, *Atmospheric Chemistry and Physics*, 16, 8593-8607,
 1404 2016.

1405 Ma, Y., Li, S., Zheng, J., Khalizov, A., Wang, X., Wang, Z., and Zhou, Y.: Size-resolved measurements of mixing state
 1406 and cloud-nucleating ability of aerosols in Nanjing, China, *Journal of Geophysical Research-Atmospheres*, 122,
 1407 9430-9450, 2017.

1408 Massling, A., Stock, M., Wehner, B., Wu, Z. J., Hu, M., Brueggemann, E., Gnauk, T., Herrmann, H., and Wiedensohler,
 1409 A.: Size segregated water uptake of the urban submicrometer aerosol in Beijing, *Atmospheric Environment*, 43,
 1410 1578-1589, 2009.

1411 Massling, A., Niedermeier, N., Hennig, T., Fors, E. O., Swietlicki, E., Ehn, M., Hameri, K., Villani, P., Laj, P., Good,
 1412 N., McFiggans, G., and Wiedensohler, A.: Results and recommendations from an intercomparison of six
 1413 Hygroscopicity-TDMA systems, *Atmospheric Measurement Techniques*, 4, 485-497, 2011.

1414 McFiggans, G., Artaxo, P., Baltensperger, U., Coe, H., Facchini, M. C., Feingold, G., Fuzzi, S., Gysel, M., Laaksonen,
 1415 A., Lohmann, U., Mentel, T. F., Murphy, D. M., O'Dowd, C. D., Snider, J. R., and Weingartner, E.: The effect of
 1416 physical and chemical aerosol properties on warm cloud droplet activation, *Atmos. Chem. Phys.*, 6, 2593-2649,
 1417 2006.

1418 McMurry, P. H., Takano, H., and Anderson, G. R.: STUDY OF THE AMMONIA (GAS) SULFURIC-ACID
 1419 (AEROSOL) REACTION-RATE, *Environmental Science & Technology*, 17, 347-352, 1983.

1420 McMurry, P. H., and Stolzenburg, M. R.: ON THE SENSITIVITY OF PARTICLE-SIZE TO RELATIVE-HUMIDITY
 1421 FOR LOS-ANGELES AEROSOLS, *Atmospheric Environment*, 23, 497-507, 1989.

1422 McMurry, P. H.: A review of atmospheric aerosol measurements, *Atmospheric Environment*, 34, 1959-1999, 2000.

1423 Meier, J., Wehner, B., Massling, A., Birmili, W., Nowak, A., Gnauk, T., Brueggemann, E., Herrmann, H., Min, H., and
 1424 Wiedensohler, A.: Hygroscopic growth of urban aerosol particles in Beijing (China) during wintertime: a
 1425 comparison of three experimental methods, *Atmospheric Chemistry and Physics*, 9, 6865-6880, 2009.

1426 Meng, J. W., Yeung, M. C., Li, Y. J., Lee, B. Y. L., and Chan, C. K.: Size-resolved cloud condensation nuclei (CCN)
 1427 activity and closure analysis at the HKUST Supersite in Hong Kong, *Atmospheric Chemistry and Physics*, 14,
 1428 10267-10282, 2014.

1429 Moore, R. H., Nenes, A., and Medina, J.: Scanning Mobility CCN Analysis-A Method for Fast Measurements of Size-
 1430 Resolved CCN Distributions and Activation Kinetics, *Aerosol Science and Technology*, 44, 861-871, 2010.

1431 Nenes, A., Chuang, P. Y., Flagan, R. C., and Seinfeld, J. H.: A theoretical analysis of cloud condensation nucleus (CCN)
 1432 instruments, *Journal of Geophysical Research-Atmospheres*, 106, 3449-3474, 2001.

1433 Otto, P., Georgii, H. W., and Bingemer, H.: A new three-stage continuous flow CCN-counter, *Atmospheric Research*,
1434 61, 299-310, 2002.

1435 Petters, M. D., and Kreidenweis, S. M.: A single parameter representation of hygroscopic growth and cloud
1436 condensation nucleus activity, *Atmospheric Chemistry And Physics*, 7, 1961-1971, 2007.

1437 Petters, M. D., Prenni, A. J., Kreidenweis, S. M., and DeMott, P. J.: On measuring the critical diameter of cloud
1438 condensation nuclei using mobility selected aerosol, *Aerosol Science and Technology*, 41, 907-913, 2007.

1439 Petters, M. D., and Kreidenweis, S. M.: A single parameter representation of hygroscopic growth and cloud
1440 condensation nucleus activity - Part 2: Including solubility, *Atmospheric Chemistry and Physics*, 8, 6273-6279,
1441 2008.

1442 Petters, M. D., Carrico, C. M., Kreidenweis, S. M., Prenni, A. J., DeMott, P. J., Collett, J. L., Jr., and Moosmueller, H.:
1443 Cloud condensation nucleation activity of biomass burning aerosol, *Journal of Geophysical Research-
1444 Atmospheres*, 114, 2009.

1445 Petters, M. D., and Kreidenweis, S. M.: A single parameter representation of hygroscopic growth and cloud
1446 condensation nucleus activity - Part 3: Including surfactant partitioning, *Atmospheric Chemistry and Physics*, 13,
1447 1081-1091, 2013.

1448 Qian, X., Zhang, Q., Xu, X., Fang, B., Zhao, W., Bao, J., and Zhang, W.: Development of a Volatility Hygroscopic
1449 Tandem Differential Mobility Analyzer (VH-TDMA) for the measurement of aerosol thermal and hygroscopic
1450 properties (in Chinese), *China Environmental Science*, 37, 1269-1275, 2017.

1451 Rader, D. J., and McMurry, P. H.: APPLICATION OF THE TANDEM DIFFERENTIAL MOBILITY ANALYZER
1452 TO STUDIES OF DROPLET GROWTH OR EVAPORATION, *Journal of Aerosol Science*, 17, 771-787, 1986.

1453 Ren, J., Zhang, F., Wang, Y., Collins, D., Fan, X., Jin, X., Xu, W., Sun, Y., Cribb, M., and Li, Z.: Using different
1454 assumptions of aerosol mixing state and chemical composition to predict CCN concentrations based on field
1455 measurements in urban Beijing, *Atmospheric Chemistry and Physics*, 18, 6907-6921, 2018.

1456 Riemer, N., Ault, A. P., West, M., Craig, R. L., and Curtis, J. H.: Aerosol Mixing State: Measurements, Modeling, and
1457 Impacts, *Reviews of Geophysics*, 57, 187-249, 2019.

1458 Roberts, G. C., and Nenes, A.: A continuous-flow streamwise thermal-gradient CCN chamber for atmospheric
1459 measurements, *Aerosol Science and Technology*, 39, 206-221, 2005.

1460 Rose, D., Gunthe, S. S., Mikhailov, E., Frank, G. P., Dusek, U., Andreae, M. O., and Poeschl, U.: Calibration and
1461 measurement uncertainties of a continuous-flow cloud condensation nuclei counter (DMT-CCNC): CCN
1462 activation of ammonium sulfate and sodium chloride aerosol particles in theory and experiment, *Atmospheric
1463 Chemistry and Physics*, 8, 1153-1179, 2008.

1464 Rose, D., Nowak, A., Achtert, P., Wiedensohler, A., Hu, M., Shao, M., Zhang, Y., Andreae, M. O., and Poeschl, U.: Cloud
1465 condensation nuclei in polluted air and biomass burning smoke near the mega-city Guangzhou, China -
1466 Part 1: Size-resolved measurements and implications for the modeling of aerosol particle hygroscopicity and
1467 CCN activity, *Atmospheric Chemistry and Physics*, 10, 3365-3383, 2010.

1468 Rose, D., Gunthe, S. S., Su, H., Garland, R. M., Yang, H., Berghof, M., Cheng, Y. F., Wehner, B., Achtert, P., Nowak,
1469 A., Wiedensohler, A., Takegawa, N., Kondo, Y., Hu, M., Zhang, Y., Andreae, M. O., and Poeschl, U.: Cloud
1470 condensation nuclei in polluted air and biomass burning smoke near the mega-city Guangzhou, China -Part 2:
1471 Size-resolved aerosol chemical composition, diurnal cycles, and externally mixed weakly CCN-active soot
1472 particles, *Atmospheric Chemistry and Physics*, 11, 2817-2836, 2011.

1473 Sinnarwalla, A. M., and Alofs, D. J.: A cloud nucleus counter with long available growth time, *Journal of Applied
1474 Meteorology*, 12, 831-835, 1973.

1475 Sjogren, S., Gysel, M., Weingartner, E., Alfarra, M. R., Duplissy, J., Cozic, J., Crosier, J., Coe, H., and Baltensperger,
1476 U.: Hygroscopicity of the submicrometer aerosol at the high-alpine site Jungfraujoch, 3580 m a.s.l., Switzerland,
1477 *Atmospheric Chemistry and Physics*, 8, 5715-5729, 2008.

1478 Snider, J. R., Petters, M. D., Wechsler, P., and Liu, P. S. K.: Supersaturation in the Wyoming CCN instrument, *Journal
1479 of Atmospheric and Oceanic Technology*, 23, 1323-1339, 2006.

1480 Stolzenburg, M. R., and McMurry, P. H.: TDMAfit User's Manual, Particle Technology Laboratory, Department of
1481 Mechanical Engineering, University of Minnesota, Minneapolis, MN 55455, 1988.

1482 Stratmann, F., Kauffeldt, T., Hummes, D., and Fissan, H.: Differential electrical mobility analysis: A theoretical study,
1483 *Aerosol Science and Technology*, 26, 368-383, 1997.

1484 Sullivan, R. C., Moore, M. J. K., Petters, M. D., Kreidenweis, S. M., Roberts, G. C., and Prather, K. A.: Effect of
1485 chemical mixing state on the hygroscopicity and cloud nucleation properties of calcium mineral dust particles,
1486 *Atmospheric Chemistry and Physics*, 9, 3303-3316, 2009.

1487 Svenssonsson, B., Rissler, J., Swietlicki, E., Mircea, M., Bilde, M., Facchini, M. C., Decesari, S., Fuzzi, S., Zhou, J.,
1488 Monster, J., and Rosenorn, T.: Hygroscopic growth and critical supersaturations for mixed aerosol particles of

1489 inorganic and organic compounds of atmospheric relevance, *Atmospheric Chemistry and Physics*, 6, 1937-1952,
1490 2006.

1491 Swietlicki, E., Hansson, H. C., Hameri, K., Svenningsson, B., Massling, A., McFiggans, G., McMurry, P. H., Petaja,
1492 T., Tunved, P., Gysel, M., Topping, D., Weingartner, E., Baltensperger, U., Rissler, J., Wiedensohler, A., and
1493 Kulmala, M.: Hygroscopic properties of submicrometer atmospheric aerosol particles measured with H-TDMA
1494 instruments in various environments - a review, *Tellus Series B-Chemical and Physical Meteorology*, 60, 432-
1495 469, 2008.

1496 Tan, H., Yin, Y., Gu, X., Li, F., Chan, P. W., Xu, H., Deng, X., and Wan, Q.: An observational study of the hygroscopic
1497 properties of aerosols over the Pearl River Delta region, *Atmospheric Environment*, 77, 817-826, 2013.

1498 Tan, H., Cai, M., Fan, Q., Liu, L., Li, F., Chan, P. W., Deng, X., and Wu, D.: An analysis of aerosol liquid water content
1499 and related impact factors in Pearl River Delta, *Science of the Total Environment*, 579, 1822-1830, 2017.

1500 Tan, W., Yu, Y., Li, C., Li, J., Kang, L., Dong, H., Zeng, L., and Zhu, T.: Profiling Aerosol Liquid Water Content Using
1501 a Polarization Lidar, *Environmental Science & Technology*, 54, 3129-3137, 2020.

1502 Tan, Z., Rohrer, F., Lu, K., Ma, X., Bohn, B., Broch, S., Dong, H., Fuchs, H., Gkatzelis, G. I., Hofzumahaus, A.,
1503 Holland, F., Li, X., Liu, Y., Liu, Y., Novelli, A., Shao, M., Wang, H., Wu, Y., Zeng, L., Hu, M., Kiendler-Scharr,
1504 A., Wahner, A., and Zhang, Y.: Wintertime photochemistry in Beijing: observations of ROx radical concentrations
1505 in the North China Plain during the BEST-ONE campaign, *Atmospheric Chemistry and Physics*, 18, 12391-12411,
1506 2018.

1507 Tang, M., Cziczo, D. J., and Grassian, V. H.: Interactions of Water with Mineral Dust Aerosol: Water Adsorption,
1508 Hygroscopicity, Cloud Condensation, and Ice Nucleation, *Chemical Reviews*, 2016.

1509 Tang, M., Huang, X., Lu, K., Ge, M., Li, Y., Cheng, P., Zhu, T., Ding, A., Zhang, Y., Gligorovski, S., Song, W., Ding,
1510 X., Bi, X., and Wang, X.: Heterogeneous reactions of mineral dust aerosol: implications for tropospheric
1511 oxidation capacity, *Atmospheric Chemistry and Physics*, 17, 11727-11777, 2017.

1512 Tang, M., Chan, C. K., Li, Y. J., Su, H., Ma, Q., Wu, Z., Zhang, G., Wang, Z., Ge, M., Hu, M., He, H., and Wang, X.:
1513 A review of experimental techniques for aerosol hygroscopicity studies, *Atmospheric Chemistry and Physics*, 19,
1514 12631-12686, 2019.

1515 Tao, J., Kuang, Y., Ma, N., Zheng, Y., Wiedensohler, A., and Zhao, C.: An improved parameterization scheme for size-
1516 resolved particle activation ratio and its application on comparison study of particle hygroscopicity measurements
1517 between HTDMA and DMA-CCNC, *Atmospheric Environment*, 226, 117403,
1518 117410.111016/j.atmosenv.112020.117403, 2020.

1519 Titos, G., Cazorla, A., Zieger, P., Andrews, E., Lyamani, H., Granados-Muñoz, M., Olmo, F., and Alados-Arboledas,
1520 L.: Effect of hygroscopic growth on the aerosol light-scattering coefficient: A review of measurements,
1521 techniques and error sources, *Atmospheric Environment*, 141, 494-507, 2016.

1522 Twomey, S.: Measurements of natural cloud nuclei, *Journal de Recherches Atmosphériques*, 1, 101-105, 1963.

1523 VanReken, T. M., Nenes, A., Flagan, R. C., and Seinfeld, J. H.: Concept for a new cloud condensation nucleus (CCN)
1524 spectrometer, *Aerosol Science and Technology*, 38, 639-654, 2004.

1525 Voutilainen, A., Stratmann, F., and Kaipio, J. P.: A non-homogeneous regularization method for the estimation of
1526 narrow aerosol size distributions, *Journal of Aerosol Science*, 31, 1433-1445, 2000.

1527 Wang, H., Lu, K., Chen, X., Zhu, Q., Chen, Q., Guo, S., Jiang, M., Li, X., Shang, D., and Tan, Z.: High N₂O₅
1528 Concentrations Observed in Urban Beijing: Implications of a Large Nitrate Formation Pathway, *Environmental
1529 Science & Technology Letters*, 2017a.

1530 Wang, J., Shen, Y., Li, K., Gao, Y., Gao, H., and Yao, X.: Nucleation-mode particle pool and large increases in N_{cn}
1531 and N_{ccn} observed over the northwestern Pacific Ocean in the spring of 2014, *Atmospheric Chemistry and
1532 Physics*, 19, 8845-8861, 2019a.

1533 Wang, Q., Yang, S., Li, Y., Yin, Y., Zhang, Z., Chen, K., and Zhao, L.: A study of multi-size aerosol hygroscopic
1534 parameterization in the summer over Huangshan Mountain (in Chinese), *Acta Meteorologica Sinica*, 74, 989-
1535 1001, 2016.

1536 Wang, T., Xue, L., Brimblecombe, P., Lam, Y. F., Li, L., and Zhang, L.: Ozone pollution in China: A review of
1537 concentrations, meteorological influences, chemical precursors, and effects, *Science of the Total Environment*,
1538 575, 1582-1596, 2017b.

1539 Wang, X., Ye, X., Chen, H., Chen, J., Yang, X., and Gross, D. S.: Online hygroscopicity and chemical measurement
1540 of urban aerosol in Shanghai, China, *Atmospheric Environment*, 95, 318-326, 2014.

1541 Wang, X., Shen, X. J., Sun, J. Y., Zhang, X. Y., Wang, Y. Q., Zhang, Y. M., Wang, P., Xia, C., Qi, X. F., and Zhong, J.
1542 T.: Size-resolved hygroscopic behavior of atmospheric aerosols during heavy aerosol pollution episodes in
1543 Beijing in December 2016, *Atmospheric Environment*, 194, 188-197, 2018a.

1544 Wang, X., Wang, X., and Yang, X.: Direct links between hygroscopicity and mixing state of ambient aerosols:
 1545 Estimating particle hygroscopicity from their single particle mass spectra, *Atmospheric Chemistry and Physics*
 1546 Discussions, 2020, 1-38, 2020a.

1547 Wang, Y., Wu, Z., and Hu, M.: Hygroscopicity of atmospheric sub-micrometer particles in various environments in
 1548 China (in Chinese), *China Environmental Science*, 37, 1601-1609, 2017c.

1549 Wang, Y., Zhang, F., Li, Z., Tan, H., Xu, H., Ren, J., Zhao, J., Du, W., and Sun, Y.: Enhanced hydrophobicity and
 1550 volatility of submicron aerosols under severe emission control conditions in Beijing, *Atmospheric Chemistry and*
 1551 *Physics*, 17, 5239-5251, 2017d.

1552 Wang, Y., Li, Z., Zhang, Y., Du, W., Zhang, F., Tan, H., Xu, H., Fan, T., Jin, X., Fan, X., Dong, Z., Wang, Q., and Sun,
 1553 Y.: Characterization of aerosol hygroscopicity, mixing state, and CCN activity at a suburban site in the central
 1554 North China Plain, *Atmospheric Chemistry and Physics*, 18, 11739-11752, 2018b.

1555 Wang, Y., Wu, Z., Ma, N., Wu, Y., Zeng, L., Zhao, C., and Wiedensohler, A.: Statistical analysis and parameterization
 1556 of the hygroscopic growth of the sub-micrometer urban background aerosol in Beijing, *Atmospheric*
 1557 *Environment*, 175, 184-191, 2018c.

1558 Wang, Y., Li, Z., Zhang, R., Jin, X., Xu, W., Fan, X., Wu, H., Zhang, F., Sun, Y., Wang, Q., Cribb, M., and Hu, D.:
 1559 Distinct Ultrafine- and Accumulation-Mode Particle Properties in Clean and Polluted Urban Environments,
 1560 *Geophysical Research Letters*, 46, 10918-10925, 2019b.

1561 Wang, Y., Chen, Y., Wu, Z., Shang, D., Bian, Y., Du, Z., Schmitt, S. H., Su, R., Gkatzelis, G. I., Schlag, P., Hohaus, T.,
 1562 Voliotis, A., Lu, K., Zeng, L., Zhao, C., Alfarra, M. R., McFiggans, G., Wiedensohler, A., Kiendler-Scharr, A.,
 1563 Zhang, Y., and Hu, M.: Mutual promotion between aerosol particle liquid water and particulate nitrate
 1564 enhancement leads to severe nitrate-dominated particulate matter pollution and low visibility, *Atmospheric*
 1565 *Chemistry and Physics*, 20, 2161-2175, 2020b.

1566 Wex, H., Petters, M., Carrico, C., Hallbauer, E., Massling, A., McMeeking, G., Poulain, L., Wu, Z., Kreidenweis, S.,
 1567 and Stratmann, F.: Towards closing the gap between hygroscopic growth and activation for secondary organic
 1568 aerosol: Part 1—Evidence from measurements, *Atmospheric Chemistry and Physics*, 9, 3987-3997, 2009.

1569 Wiedensohler, A., Cheng, Y. F., Nowak, A., Wehner, B., Achtert, P., Berghof, M., Birmili, W., Wu, Z. J., Hu, M., Zhu,
 1570 T., Takegawa, N., Kita, K., Kondo, Y., Lou, S. R., Hofzumahaus, A., Holland, F., Wahner, A., Gunthe, S. S., Rose,
 1571 D., Su, H., and Poeschl, U.: Rapid aerosol particle growth and increase of cloud condensation nucleus activity
 1572 by secondary aerosol formation and condensation: A case study for regional air pollution in northeastern China,
 1573 *Journal of Geophysical Research-Atmospheres*, 114, D00G08, 10.1029/2008JD010884, 2009.

1574 Wu, Y., Yin, Y., Gu, X., and Tan, H.: An observational study of the hygroscopic properties of aerosols in north suburb
 1575 of Nanjing (in Chinese), *China Environmental Science*, 34, 1938-1949, 2014.

1576 Wu, Y., Qiu, Y., Guo, J., Wang, K., Wang, J., and Zhou, X.: An Observational Study on the Hygroscopic Properties of
 1577 Aerosol Particles at Different AltitudesA Case Study in the Mt. Huangshan (in Chinese), *Resources and*
 1578 *Environment in the Yangtze Basin*, 27, 1361-1370, 2018a.

1579 Wu, Z., Zheng, J., Wang, Y., Shang, D., Du, Z., Zhang, Y., and Hu, M.: Chemical and physical properties of biomass
 1580 burning aerosols and their CCN activity: A case study in Beijing, China, *Science of the Total Environment*, 579,
 1581 1260-1268, 2017.

1582 Wu, Z., Chen, J., Wang, Y., Zhu, Y., Liu, Y., Yao, B., Zhang, Y., and Hu, M.: Interactions between water vapor and
 1583 atmospheric aerosols have key roles in air quality and climate change, *National Science Review*, 5, 452-454,
 1584 2018b.

1585 Wu, Z. J., Nowak, A., Poulain, L., Herrmann, H., and Wiedensohler, A.: Hygroscopic behavior of atmospherically
 1586 relevant water-soluble carboxylic salts and their influence on the water uptake of ammonium sulfate, *Atmospheric*
 1587 *Chemistry and Physics*, 11, 12617-12626, 2011.

1588 Wu, Z. J., Zheng, J., Shang, D. J., Du, Z. F., Wu, Y. S., Zeng, L. M., Wiedensohler, A., and Hu, M.: Particle
 1589 hygroscopicity and its link to chemical composition in the urban atmosphere of Beijing, China, during
 1590 summertime, *Atmospheric Chemistry and Physics*, 16, 1123-1138, 2016.

1591 Xie, Y., Ye, X., Ma, Z., Tao, Y., Wang, R., Zhang, C., Yang, X., Chen, J., and Chen, H.: Insight into winter haze
 1592 formation mechanisms based on aerosol hygroscopicity and effective density measurements, *Atmospheric*
 1593 *Chemistry and Physics*, 17, 7277-7290, 2017.

1594 Xu, B.: Hygroscopic properties of aerosol particles in Nanjing and Mount Huangshan (in Chinese), Master of Science,
 1595 School of Atmospheric Physics, Nanjing University of Information Science and Technology, Nanjing, China, 31-
 1596 45 pp., 2015.

1597 Xu, B., Zhang, Z.-f., Li, Y.-w., Qin, X., Miao, Q., and Shen, Y.: Hygroscopic Properties of Aerosol Particles in North
 1598 Suburb of Nanjing in Spring (in Chinese), *Huan jing ke xue= Huanjing kexue*, 36, 1911-1918, 2015.

1599 Yan, Y., Fu, P., Jing, B., Peng, C., Boreddy, S. K. R., Yang, F., Wei, L., Sun, Y., Wang, Z., and Ge, M.: Hygroscopic
 1600 behavior of water-soluble matter in marine aerosols over the East China Sea, *Science of the Total Environment*,
 1601 578, 307-316, 2017.

1602 Yang, F., Xue, H., Deng, Z., Zhao, C., and Zhang, Q.: A closure study of cloud condensation nuclei in the North China
 1603 Plain using droplet kinetic condensational growth model, *Atmospheric Chemistry and Physics*, 12, 5399-5411,
 1604 2012.

1605 Yang, S., Tian, Z., Zhang, T., Yu, X., Li, Y., An, J., Zhao, X., Li, Y., Wang, Z., and Wu, S.: Urban Aerosol
 1606 Hygroscopicity During Haze Weather (in Chinese), *Environmental Science*, 40, 2546-2555, 2019.

1607 Yao, X., Lau, N. T., Fang, M., and Chan, C. K.: Correlations of ambient temperature and relative humidity with
 1608 submicron particle number concentration size distributions in on-road vehicle plumes, *Aerosol Science and*
 1609 *Technology*, 41, 692-700, 2007.

1610 Ye, X., Ma, Z., Hu, D., Yang, X., and Chen, J.: Size-resolved hygroscopicity of submicrometer urban aerosols in
 1611 Shanghai during wintertime, *Atmospheric Research*, 99, 353-364, 2011.

1612 Ye, X., Tang, C., Yin, Z., Chen, J., Ma, Z., Kong, L., Yang, X., Gao, W., and Geng, F.: Hygroscopic growth of urban
 1613 aerosol particles during the 2009 Mirage-Shanghai Campaign, *Atmospheric Environment*, 64, 263-269, 2013.

1614 Yeung, M. C., Lee, B. P., Li, Y. J., and Chan, C. K.: Simultaneous HTDMA and HR-ToF-AMS measurements at the
 1615 HKUST Supersite in Hong Kong in 2011, *Journal of Geophysical Research-Atmospheres*, 119, 9864-9883, 2014.

1616 Zhang, F., Li, Y., Li, Z., Sun, L., Li, R., Zhao, C., Wang, P., Sun, Y., Liu, X., Li, J., Li, P., Ren, G., and Fan, T.: Aerosol
 1617 hygroscopicity and cloud condensation nuclei activity during the AC(3)Exp campaign: implications for cloud
 1618 condensation nuclei parameterization, *Atmospheric Chemistry and Physics*, 14, 13423-13437, 2014.

1619 Zhang, F., Li, Z., Li, Y., Sun, Y., Wang, Z., Li, P., Sun, L., Wang, P., Cribb, M., Zhao, C., Fan, T., Yang, X., and Wang,
 1620 Q.: Impacts of organic aerosols and its oxidation level on CCN activity from measurement at a suburban site in
 1621 China, *Atmospheric Chemistry and Physics*, 16, 5413-5425, 2016a.

1622 Zhang, F., Wang, Y., Peng, J., Ren, J., Collins, D., Zhang, R., Sun, Y., Yang, X., and Li, Z.: Uncertainty in Predicting
 1623 CCN Activity of Aged and Primary Aerosols, *Journal of Geophysical Research-Atmospheres*, 122, 11723-11736,
 1624 2017.

1625 Zhang, F., Ren, J., Fan, T., Chen, L., Xu, W., Sun, Y., Zhang, R., Liu, J., Jiang, S., Jin, X., Wu, H., Li, S., Cribb,
 1626 M. C., and Li, Z.: Significantly Enhanced Aerosol CCN Activity and Number Concentrations by Nucleation-Initiated
 1627 Haze Events: A Case Study in Urban Beijing, *Journal of Geophysical Research-Atmospheres*, 124, 14102-14113,
 1628 2019a.

1629 Zhang, J., Wang, L., Chen, J., Feng, S., Shen, J., and Jiao, L.: Hygroscopicity of ambient submicron particles in urban
 1630 Hangzhou, China, *Frontiers of Environmental Science & Engineering in China*, 5, 342-347, 2011.

1631 Zhang, Q., Meng, J., Quan, J., Gao, Y., Zhao, D., Chen, P., and He, H.: Impact of aerosol composition on cloud
 1632 condensation nuclei activity, *Atmospheric Chemistry and Physics*, 12, 3783-3790, 2012.

1633 Zhang, Q., Zheng, Y., Tong, D., Shao, M., Wang, S., Zhang, Y., Xu, X., Wang, J., He, H., Liu, W., Ding, Y., Lei, Y., Li,
 1634 J., Wang, Z., Zhang, X., Wang, Y., Cheng, J., Liu, Y., Shi, Q., Yan, L., Geng, G., Hong, C., Li, M., Liu, F., Zheng,
 1635 B., Cao, J., Ding, A., Gao, J., Fu, Q., Huo, J., Liu, B., Liu, Z., Yang, F., He, K., and Hao, J.: Drivers of improved
 1636 PM2.5 air quality in China from 2013 to 2017, *Proceedings of the National Academy of Sciences of the United*
 1637 *States of America*, 116, 24463-24469, 2019b.

1638 Zhang, R., Wang, G., Guo, S., Zarnora, M. L., Ying, Q., Lin, Y., Wang, W., Hu, M., and Wang, Y.: Formation of Urban
 1639 Fine Particulate Matter, *Chemical Reviews*, 115, 3803-3855, 2015.

1640 Zhang, R., Tang, L., Xu, H., Du, S., Qin, W., Jiang, L., Tan, H., Liu, J., and Yang, Y.: Hygroscopic properties of urban
 1641 aerosol in Nanjing during wintertime (in Chinese), *Acta Scientiae Circumstantiae*, 38, 32-40, 2018.

1642 Zhang, S. L., Ma, N., Kecorius, S., Wang, P. C., Hu, M., Wang, Z. B., Groess, J., Wu, Z. J., and Wiedensohler, A.:
 1643 Mixing state of atmospheric particles over the North China Plain, *Atmospheric Environment*, 125, 152-164,
 1644 2016b.

1645 Zhang, X., Xu, X., Ding, Y., Liu, Y., Zhang, H., Wang, Y., and Zhong, J.: The impact of meteorological changes from
 1646 2013 to 2017 on PM2.5 mass reduction in key regions in China, *Science China-Earth Sciences*, 62, 1885-1902,
 1647 2019c.

1648 Zhao, C., Yu, Y., Kuang, Y., Tao, J., and Zhao, G.: Recent Progress of Aerosol Light-scattering Enhancement Factor
 1649 Studies in China, *Advances in Atmospheric Sciences*, 36, 1015-1026, 2019.

1650 Zhu, T., Shang, J., and Zhao, D.: The roles of heterogeneous chemical processes in the formation of an air pollution
 1651 complex and gray haze, *Science China Chemistry*, 54, 145-153, 2011.

1652 Zhu, Y., Li, K., Shen, Y., Gao, Y., Liu, X., Yu, Y., Gao, H., and Yao, X.: New particle formation in the marine
 1653 atmosphere during seven cruise campaigns, *Atmospheric Chemistry and Physics*, 19, 89-113, 2019.

1654 Zieger, P., Vaisanen, O., Corbin, J. C., Partridge, D. G., Bastelberger, S., Mousavi-Fard, M., Rosati, B., Gysel, M.,
1655 Krieger, U. K., Leck, C., Nenes, A., Riipinen, I., Virtanen, A., and Salter, M. E.: Revising the hygroscopicity of
1656 inorganic sea salt particles, *Nature Communications*, 8, 2017.
1657